*Mineralogical Magazine, December 2014, Vol. 78(7), pp. 1527–1552*

# The crystal structure of camerolaite and structural variation in the cyanotrichite family of merotypes

S. J. Mills[1,*], A. G. Christy[2], C. Schnyder[3], G. Favreau[4] and J. R. Price[5]

[1] Geosciences, Museum Victoria, GPO Box 666, Melbourne, Victoria 3001, Australia
[2] Centre for Advanced Microscopy, Australian National University, Canberra, ACT 0200, Australia
[3] Département de minéralogie et de pétrographie, Muséum d'histoire naturelle, 1 rte de Malagnou, Case postale 6434, CH - 1211 Genève 6, Switzerland
[4] 421 Avenue Jean Monnet, 13090 Aix-en-Provence, France
[5] Australian Synchrotron, 800 Blackburn Road, Clayton, Victoria 3168, Australia

[*Received 25 March 2014; Accepted 15 May 2014; Associate Editor: S. Krivovichev*]

**ABSTRACT**

We present Raman data for camerolaite, cyanotrichite and carbonatecyanotrichite, and using synchrotron single-crystal X-ray diffraction have solved the structure of camerolaite from the Tistoulet Mine, Padern, Aude Department, France. Camerolaite crystallizes in space group $P1$ with the unit-cell parameters: $a = 6.3310(13)$ Å, $b = 2.9130(6)$ Å, $c = 10.727(2)$ Å, $\alpha = 93.77(3)^o$, $\beta = 96.34(3)^o$, $\gamma = 79.03(3)^o$, $V = 192.82(7)$ Å$^3$ and $Z = ⅓$, with respect to the ideal formula from the refinement, $Cu_6Al_3(OH)_{18}(H_2O)_2[Sb(OH)_6](SO_4)$. The crystal structure was solved to $R_1 = 0.0890$ for all 1875 observed reflections [$F_o > 4\sigma F_o$] and 0.0946 for all 2019 unique reflections. The $P$ cell has been transformed into a $C$-centred cell that aids comparison with that of the structurally related khaidarkanite by $\mathbf{a}_C = 2\mathbf{a}_P - \mathbf{b}_P$, giving parameters $a = 12.441(3)$, $b = 2.9130(6)$, $c = 10.727(2)$ Å, $\alpha = 93.77(3)$, $\beta = 95.57(3)$, $\gamma = 92.32(3)^o$ and $Z = ⅔$ in $C1$. Edge-sharing octahedral ribbons $Cu_2Al(O,OH,H_2O)_8$ form hydrogen-bonded layers ∥ (001), as in khaidarkanite. The partially occupied interlayer Sb and S sites of the average structure are in octahedral and tetrahedral coordination by oxygen, respectively. They cannot be occupied simultaneously, which leads to regular alternation of $[Sb(OH)_6]^-$ and $SO_4^{2-}$ groups in rods ∥ **y**, resulting in local tripling of the periodicity along **y** for the $Sb(OH)_6-SO_4$ rods. Thus, camerolaite has a 'host–guest' structure in which an invariant host module (layers of Cu–Al ribbons) has embedded rod-like guest modules with a longer periodicity. Coupling between the phases of these rods is only short-range, resulting in diffuse X-ray scattering rather than sharp superstructure reflections. Similar disorder is known for parnauite, and is deduced for other members of the cyanotrichite group (cyanotrichite, carbonatecyanotrichite and khaidarkanite). Group members all share the Cu–Al ribbon module but have interlayer rods of different compositions and topologies; thus, they form a merotypic family. The low symmetry of the camerolaite average structure suggests other possibilities for structure variation in the group, which are discussed.

**Keywords:** camerolaite, cyanotrichite, carbonatecyanotrichite, khaidarkanite, merotype, superstructure, crystal structure, synchrotron.

## Introduction

The blue, acicular minerals of the cyanotrichite group have been known for more than two centuries, but their structural and chemical complexities continue to defy full characterization. The state of the art regarding cyanotrichite *sensu stricto*, carbonatecyanotrichite, khaidarkanite, camerolaite and possible new group members was reviewed thoroughly by Hager *et al*. (2009). At that time, only the structure of

* E-mail: smills@museum.vic.gov.au
DOI: 10.1180/minmag.2014.078.7.02

khaidarkanite had been refined, although the similar unit-cell parameters for all group members implied similarity of the major features of the structures.

Samples have been examined from three different museum collections for examples of group members that were of sufficient quality for additional structure refinement using synchrotron X-ray diffraction (XRD). Raman spectral data are presented for seven examples of camerolaite, one of carbonatecyanotrichite and two of cyanotrichite. Only camerolaite from one locality, the Tistoulet Mine, Padern, Aude Department, France, was found to occur in crystals large enough for a structure refinement to be possible, which is also presented here.

## Occurrence

The Corbières massif, south of the Aude Department, Languedoc-Roussillon, France, hosts many small mines operated mainly in the second half of the 19$^{th}$ century and first half of the 20$^{th}$ century, chiefly for copper and baryte. The Padern–Montgaillard district (60 km southwest of Narbonne, 70 km southeast of Carcassonne) is the richest area, as far as mineral species are concerned, and has been studied extensively since the 1980s by Association Française de Microminéralogie (Deliens *et al.*, 1993; Berbain *et al.*, 2005).

The Tistoulet mine, 4 km north of the village of Padern, has been operated sporadically from Roman times up to 1929. It consists of three east-west trending, parallel quartz veins in Lower Devonian limestone and dolomite (Esquine d'Ase, Tistoulet, Causseille). Only the first ('Esquine d'Ase' or 'donkey backbone') vein has been heavily worked. The main mineralization (Hg- and Ag-rich fahlore) is scattered in irregular masses, which has resulted in some 700 m of galleries being excavated, and 15–20 thousand tons of raw ore extracted from the rich part of the vein, then hauled *via* cable to a processing plant equipped with crushers and shaking screens (destroyed in 1990).

Operations were carried out at several levels, named after their elevation, and corresponding to adits or mineralized outcrops. Mineralogical study of these levels resulted in the description of several distinct mineral suites and a total of ~80 species. The most significant levels are Level 384 (Cu sulfates, native Ag and cuprite), Level 430 (Cu, Pb, Zn and Fe arsenates) and Level 470 (cyanotrichite, camerolaite and cualstibite). The specimen studied was collected by GF on the dumps of Level 470 in 2002 and has been deposited in the collections of the Geosciences department, Museum Victoria, as specimen number M52913. The host rock is fine-grained white quartz with minor carbonates (azurite and malachite) and oxyplumboroméite, generally devoid of any primary metallic minerals, and locally rich in cyanotrichite/camerolaite. Arsenates are rare, generally limited to pharmacosiderite and olivenite. Cualstibite was identified in this environment for the second time in France (Favreau *et al.*, 2003). Camerolaite and cyanotrichite occur in needles, reaching 1 mm long and are organized generally as sprays or balls (Fig. 1). Cyanotrichite is typically pale blue; while camerolaite may be greyish green, pale blue or vivid blue. The crystals of camerolaite are remarkable for their thickness and distinct terminations, and are undoubtedly the best for the species. The unique thickness of the crystals has enabled the structure to be determined in this present study.

## Experimental

### *Samples*

Samples analysed in this study come from the collections of the Geosciences department, Museum Victoria, Australia (M), Département de minéralogie et de pétrographie, Muséum d'histoire naturelle, Geneva, Switzerland (MHNG) and Musée Cantonal de Géologie, Lausanne, Switzerland (MGL). It should be noted that Sarp and Perroud (1991) did not publish the holotype number of camerolaite

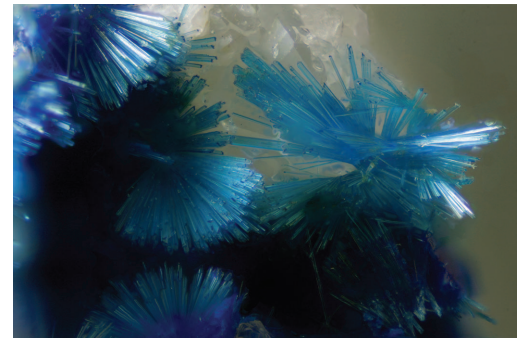

FIG. 1. Intergrown crystals of camerolaite from Padern. Field of view 2 mm across. Georges Favreau specimen, Pierre Clolus photograph.

from Cap Garonne in their paper, but subsequently transmitted the provisory museum number MHNG 435/84 to the Commission on Museums, which was then published in Anthony *et al.* (2003). This number was then replaced by 477.067, and the sample placed into the holotype section of the museum.

### *Spectroscopy*

The Raman spectra were obtained over the 4000–100 $cm^{-1}$ range. Data were collected with a Renishaw inVia spectrometer coupled with a Leica DM2500 microscope. Calibration was made using the 521 $cm^{-1}$ line of elemental silicon. Two lasers were used for this study: Nd-YAG laser at 532 nm and Diode laser at 785 nm. During the analyses, power ranging from 5 to 30 mW was applied to the samples. Each analysis was conducted on a single acicular crystal taken from a radiating aggregate, with the laser beam orthogonal to the elongation direction of the crystal (*b* axis). Representative spectra are shown in Fig. 2 and bands with assignments in Table 1.

The infrared (IR) spectra were obtained using a Bruker Alpha FTIR with a diamond Attenuated Total Reflectance attachment (ATR), DTGS (Deuterated Triglycine Sulfate) detector, 4 $cm^{-1}$ resolution and 4000–450 $cm^{-1}$ range. The samples were placed on the ATR crystal and pressure exerted by screwing the pressure clamp onto the sample to ensure maximum contact with the ATR crystal. Thirty-two scans were taken for each item and co-added.

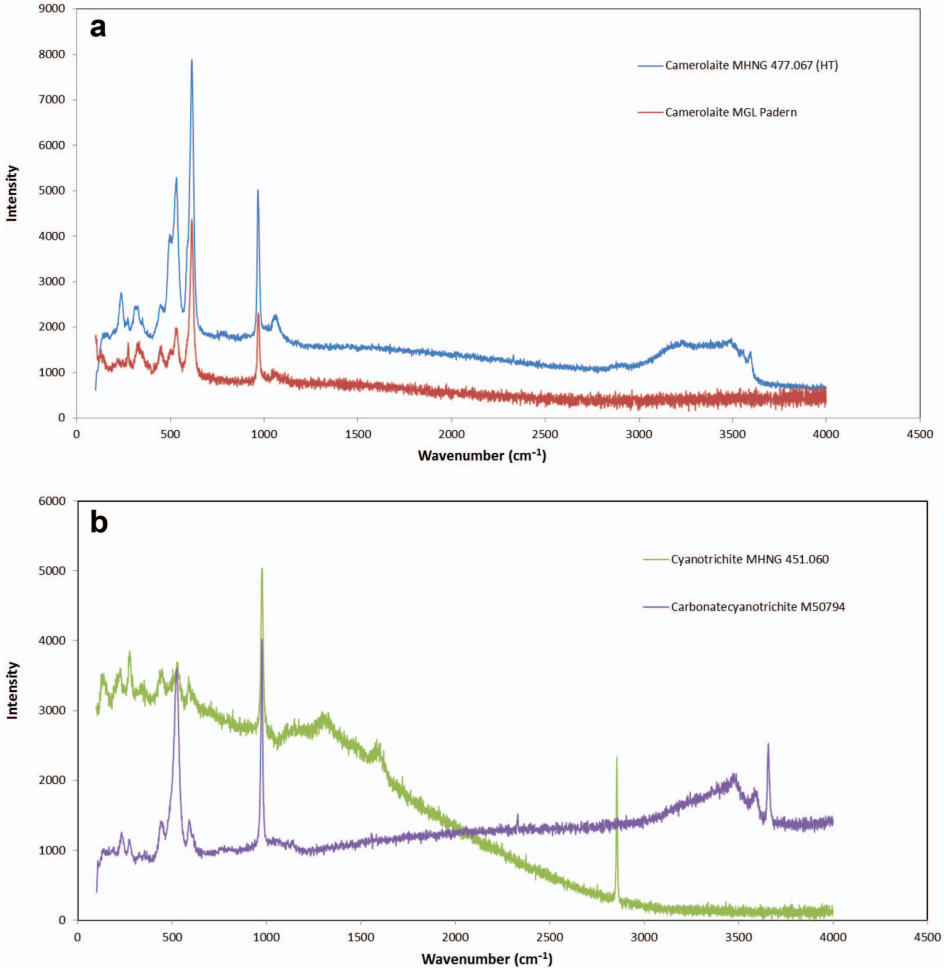


FIG. 2. Raman spectra for (*a*) camerolaite and (*b*) cyanotrichite and carbonatecyanotrichite.

TABLE 1.Raman data for camerolaite, cyanotrichite and carbonatecyanotrichite.

| Mineral name | Camerolaite | Camerolaite | Camerolaite | Camerolaite |
|---|---|---|---|---|
| Museum number | MHNG 477.067 (HT) | MHNG 388.045 | MGL 9/1/202 | MGL Padern |
| Locality | Cap Garonne | Cap Garonne | Les Moulins | Padern |
| Lattice mode | – | – | – | 216 w-br |
| Lattice mode | 237 m | 236 w | 230 w | – |
| Lattice mode | 272 m | 274 vw | 274 w | 274 m |
| Lattice mode | 325 m | 325 vw | 330 w-br | 333 m-br |
| Lattice mode | 347 vw | – | – | – |
| $\nu_2$ ($SO_4$) | 447 m-br | 444 w-br | 440 w | 444 m-br |
| $\nu_4$ ($SO_4$) | 526 vs | 524 s | 527 m | 531 m |
| $\nu_4$ ($SO_4$) | 614 vs | 613 m | 615 vs | 614 vs |
| $\nu_1$ ($SO_4$) | 968 s | 976 vs | 969 s | 969 s |
| $\nu_3$ ($SO_4$) | 1050 vvw-vbr | 1049 w-br | 1050 vw-vbr | 1049 vw-vbr |
| $\nu_3$ ($SO_4$) | 1064 w-br | 1061 w-br | – | – |
| H–O–H bending | – | 1600 w-vbr | – | – |
| ? Stretching mode of $H_2O$ | 2330 vw | 2529 w | – | – |
| Stretching mode of $H_2O$ | – | – | 2986 w-vbr | – |
| Stretching mode of $H_2O$ | 3100–3200 m-vvbr | 3100–3300 w-vbr | – | – |
| Stretching mode of OH | 3495 m-vbr | | – | – |
| Stretching mode of OH | 3558 m-vbr | 3560 m | – | – |
| Stretching mode of OH | 3596 m-br | 3575 m | – | – |
| Stretching mode of O | – | – | – | – |
| Operating Parameters | 532nm 30s, 5%, 1acc, L100x | 532nm 30s, 5%, 1acc, L100x | 785nm 25s, 5%, 5acc, L50x | 785nm 25s, 5%, 5acc, L100x |

| Mineral name | Cyanotrichite | Carbonatecyanotrichite | Cyanotrichite | Camerolaite | Camerolaite |
|---|---|---|---|---|---|
| Museum number | M50793 | M50794 | MHNG 451.060 | M52913 | M4616 |
| Locality | Grandview mine | Grandview mine | Cap Garonne | Padern | Cap Garonne |
| Lattice mode | 230w | 233w | 227 w-br | 237w | 237w-br |
| Lattice mode | – | – | – | – | – |
| Lattice mode | 274w | 273w | 275 m-br | 274vw | 273w |
| Lattice mode | – | – | – | 325w-br | 328vw |
| Lattice mode | – | – | 338 vw-br | – | 351vw |
| $\nu_2$ ($SO_4$) | 448m | 441m | 447 w-br | 447vw | 446w |
| $\nu_4$ ($SO_4$) | 525s | 524vs | 527 m-br | 493–525m (doublet) | 528m |
| $\nu_4$ ($SO_4$) | 592m | 591m | 588 m-br | – | – |

| | | | | | | | | | | | | | | |
|---|---|---|---|---|---|---|---|---|---|---|---|---|---|---|
| $\nu_1$ ($SO_4$) | 609vw | – | – | 613s | | | | | | | 613s | | | |
| $\nu_3$ ($SO_4$) | 977 vs | 977vs | 976 vs | 967m | | | | | | | (968)–978vs (doublet) | | | |
| $\nu_3$ ($SO_4$) | – | – | – | – | | | | | | | 1072vw | | | |
| $\nu_3$ ($SO_4$) | 1142vw | 1141w-br | – | – | | | | | | | – | | | |
| H–O–H bending | – | – | – | – | | | | | | | 1560–1580vw-vbr | | | |
| ? Stretching mode of $H_2O$ | 2330vw | 2329w | 2852 vs | – | | | | | | | – | | | |
| Stretching mode of OH | – | – | – | 3100–3250-vbr | | | | | | | – | | | |
| Stretching mode of OH | 3300–3400m-vbr | 3300–3400m-vvbr | – | 3500m-br | | | | | | | – | | | |
| Stretching mode of OH | 3590m-vbr | 3583m-br | – | 3550m-br | | | | | | | 3593m | | | |
| Stretching mode of OH | – | 3657m | 3777 vvw | 3594m | | | | | | | – | | | |
| Operating parameters | 532nm | 20s, | 5%, | 2 acc, | 532nm | 20s, | 5%, | 2acc, | 785nm | 30s, | 10%, | 1acc, | 532nm | 20s, | 5%, | 2acc, | 532nm | 20s, | 5%, | 2acc, |
| | L100x | | | | L100x | | | | L50x | | | | L100x | | | | L100x | | | |

### *Single-crystal X-ray diffraction*

Exceptionally large, good-quality crystals from the Tistoulet Mine were examined by qualitative energy-dispersive spectroscopy, which showed the presence of only Cu, Al, Sb and S as major cations, identifying them as camerolaite. A 70 μm × 10 μm × 10 μm needle of camerolaite was mounted on a nylon loop to minimize diffraction from the sample mount for an X-ray data collection on the micro-focus macromolecular beam line MX2 of the Australian Synchrotron. Data were collected at 100 K using an ADSC Quantum 315r detector and monochromatic radiation with a wavelength of 0.7093 Å. A φ scan was employed with frame widths of 1º and a counting time per frame of 1 s. The e-statistics gave the mean $|E^2-1| = 0.783$, indicating a non-centrosymmetric space group, so the intensity data sets were processed in *P*1 using *XDSauto* (Kabsch, 2010) and *SADABS* (Bruker, 2001), giving 3816 reflections with an $R_{int}$ of 0.0627. Racemic twinning (55:45) was identified in the dataset. The heavy Cu and Al atoms were found using *SHELXS-97* (Sheldrick, 2008). All other atoms were then located *via* subsequent difference-Fourier syntheses during the refinement, performed using *SHELXL-97* (Sheldrick, 2008). Details concerning data collection and structure refinement are provided in Table 2. Fractional coordinates and atom displacement parameters are provided in Table 3.

Initial refinement of the S and Sb sites showed that they were not fully occupied. Furthermore, sites O7–O10 needed to be split, as indicated by the thermal parameters and also so as to optimize the coordination around these cations, as discussed in detail below. Modelling of possible short-range ordered configurations (see below) showed that in the maximally ordered case, each of the sites could have only 17%, 33%, 67% or 83% occupancy. They were then fixed at these values (Table 3). The positions of the O7–O10 and S sites were fixed in the final refinement due to their extremely low occupancies, and the thermal parameters for each split site were constrained to be equal to each other. The final model, with all atoms isotropically refined, converged to $R_1 = 0.0890$ for all 1875 observed reflections [$F_o > 4\sigma F_o$] and 0.0946 for all 2019 unique reflections. Diffuse reflections were observed that corresponded to an incipient 3*b* superstructure. These are interpreted as corresponding to a local tripling of the structure

TABLE 2. Data collection and structure refinement details for camerolaite.

| | |
|---|---|
| Structural Formula | $Cu_6Al_3(OH)_{18}(H_2O)_2[Sb(OH)_6](SO_4)$ |
| Space group | $P\bar{1}$ |
| Unit-cell parameters | |
| $a$ (Å) | 6.3310(13) |
| $b$ (Å) | 2.9130(6) |
| $c$ (Å) | 10.727(2) |
| α (°) | 93.77(3) |
| β (°) | 96.34(3) |
| γ (°) | 79.03(3) |
| $V$ | 192.82(7) |
| $Z$ | ⅓ |
| Temperature | 100(2) K |
| Absorption coefficient | 9.570 $mm^{-1}$ |
| $F(000)$ | 202 |
| ° range | 1.91−32.84 |
| Index ranges | |
| $h$ | $-9 \leqslant h \leqslant 9$ |
| $k$ | $-4 \leqslant k \leqslant 4$ |
| $l$ | $-15 \leqslant l \leqslant 15$ |
| Reflections collected | 3811 |
| Reflections with $F > 4\sigma(F)$ | 2019 |
| Refinement method | Full-matrix least-squares on $F^2$ |
| Parameters refined | 49 |
| Gof | 1.095 |
| Final $R$ indices [$F_o > 4\sigma(F)$] | $R_1 = 0.0890$, w$R_2 = 0.0946$ |
| $R$ indices (all data) | $R_1 = 0.2233$, w$R_2 = 0.2285$ |
| Largest diff. peak / hole | 2.417 / −3.229 $e$/Å$^3$ |

TABLE 3. Atom coordinates and displacement parameters (Å$^2$) for camerolaite.

| Atom | $x$ | $y$ | $z$ | Occupancy | $U_{eq}$ |
|---|---|---|---|---|---|
| Al1 | −0.0194(16) | 0.039(4) | −0.0179(11) | 1 | 0.0077(6) |
| Cu1 | 0.3082(13) | 0.441(3) | 0.1807(8) | 1 | 0.0119(5) |
| Cu2 | 0.6368(13) | 0.629(3) | 0.7830(8) | 1 | 0.0089(4) |
| O1 | 0.861(2) | 0.033(5) | 0.8078(13) | 1 | 0.0004(19) |
| O2 | 0.096(3) | 0.007(6) | 0.1560(18) | 1 | 0.020(3) |
| O3 | 0.440(2) | 0.212(5) | 0.7778(14) | 1 | 0.004(2) |
| O4 | 0.526(3) | 0.854(7) | 0.1876(18) | 1 | 0.020(3) |
| O5 | 0.155(2) | 0.444(6) | 0.9574(15) | 1 | 0.009(2) |
| O6 | 0.779(2) | 0.609(6) | 0.0041(16) | 1 | 0.011(3) |
| O7a | 0.657 | 0.565 | 0.531 | 0.17 | 0.035(4) |
| O7b | 0.681 | 0.73 | 0.526 | 0.17 | 0.035(4) |
| O7o | 0.618 | 0.617 | 0.547 | 0.67 | 0.035(4) |
| O8a | 0.912 | 0.88 | 0.47 | 0.17 | 0.025(3) |
| O8b | 0.851 | 0.093 | 0.376 | 0.17 | 0.025(3) |
| O8o | 0.879 | 0.091 | 0.356 | 0.67 | 0.025(3) |
| O9a | 0.229 | 0.05 | 0.587 | 0.17 | 0.017(3) |
| O9b | 0.008 | 0.047 | 0.582 | 0.17 | 0.017(3) |
| O9o | 0.098 | 0.025 | 0.602 | 0.67 | 0.017(3) |
| O10a | 0.125 | 0.285 | 0.37 | 0.17 | 0.019(2) |
| O10o | 0.247 | 0.476 | 0.405 | 0.83 | 0.019(2) |
| Sb1 | 0.9722(14) | 0.517(3) | 0.4822(9) | 0.33 | 0.0099(4) |
| S1 | 0.142 | 0.909 | 0.46 | 0.16 | 0.001(3) |
| S2 | 0.8 | 0.105 | 0.509 | 0.17 | 0.030(6) |

TABLE 4. Selected bond distances (Å) in camerolaite.

| | | | | | |
|---|---|---|---|---|---|
| Al1 | O5 | 1.812(14) | Cu2 | O3 | 1.893(11) |
| | O6 | 1.910(15) | | O3 | 1.906(12) |
| | O1 | 1.939(13) | | O1 | 1.995(11) |
| | O5 | 1.890(14) | | O1 | 2.034(10) |
| | O2 | 1.928(19) | | O6 | 2.443(14) |
| | O6 | 1.992(14) | | O7o | 2.519(14) |
| | <Al−O> | 1.912 | | <Cu−O> | 2.132 |
| | σ(Al−O) | 0.060 | | σ(Cu−O) | 0.277 |
| Cu1 | O2 | 1.931(15) | Sb | O8o | 1.898(10) |
| | O4 | 1.982(17) | | O9o | 1.981(9) |
| | O4 | 1.989(16) | | O10o | 1.988(9) |
| | O2 | 1.999(17) | | O9o | 2.109(10) |
| | O10o | 2.471(17) | | O8o | 2.172(9) |
| | O5 | 2.483(17) | | O7o | 2.381(9) |
| | <Cu−O> | 2.143 | | <Sb−O> | 2.088 |
| | σ(Cu−O) | 0.260 | | σ(Sb−O) | 0.174 |

periodicity in the immediate environment of the Sb, S and split oxygen positions, which is discussed below.

Selected interatomic distances are shown in Table 4. These include distances from cations to the highest-occupancy split sites O7o (67% occupied) and O10o (83% occupied). It can be seen that Cu1 and Cu2 are in 4+2 coordination, surrounded by the typical Jahn−Teller distorted elongated octahedra, while the Al are surrounded by much more regular octahedra. The bond-valence parameters of Brese and O'Keeffe (1991) give bond-valence sums of 2.03, 2.14 and 3.00 valence units for Cu1, Cu2 and Al, respectively, which are all reasonable. The Sb octahedron is highly distorted, as discussed below.

## Discussion

### *Raman and infrared spectroscopy*

The Raman data for camerolaite, cyanotrichite and carbonatecyanotrichite from a number of samples are shown in Table 1. The majority of bands observed are found in all three phases and include: $\nu_2$ ($SO_4$) observed at ~440 $cm^{-1}$, $\nu_4$ ($SO_4$) observed at ~525, 590 and 610 $cm^{-1}$, $\nu_1$ ($SO_4$) at 970 $cm^{-1}$ and $\nu_3$ ($SO_4$) observed between 1050−1140 $cm^{-1}$ The positioning of these bands is very similar to that observed in parnauite (Mills *et al*., 2013). In the carbonate-cyanotrichite sample M50794 (corresponding to PAWCYAN of Hager *et al*., 2009), no bands corresponding to $CO_3$ were observed. However, note that IR spectroscopy is a more sensitive method for the detection of carbonate groups, and in fact, bands are observed at 1036, 1093, 1389 and 1505 $cm^{-1}$ (Fig. 3). Cyanotrichite sample M50793 (corresponding to GRAND of Hager *et al*., 2009) showed bands at 1035 and 1093 $cm^{-1}$ but no additional significant features in the 1300−1600 $cm^{-1}$ region, supporting the conclusions of Hager *et al*. (2009). While bands at or near 1036 and 1093 $cm^{-1}$ can occur for both $SO_4$ and $CO_3$, the bands at 1389 and 1505 $cm^{-1}$ can thus be attributed specifically to $CO_3$ antisymmetric stretching modes. In particular, the band at 1389 $cm^{-1}$ may be assigned to the $CO_3$ antisymmetric stretching mode of a $CO_3$ anion hydrogen-bonded to a $H_2O$ molecule. The band at 1646 $cm^{-1}$, also indicated in Fig. 3, is a H−O−H bending mode of an $H_2O$ molecule. This band was present for both M50793 and M50794.

### *Shared structural features of the cyanotrichite-group structures*

Hager *et al*. (2009) proposed that cyanotrichite, carbonatecyanotrichite, camerolaite and khaidarkanite, and some possible new minerals, formed a structural group based on similarities in their stoichiometry and unit-cell parameters. At that time, khaidarkanite was the only one of these minerals for which the crystal structure had been refined (Rastsvetaeva *et al*., 1997; Hager *et al*., 2009). The structure presented in the present study for camerolaite confirms the close relation-

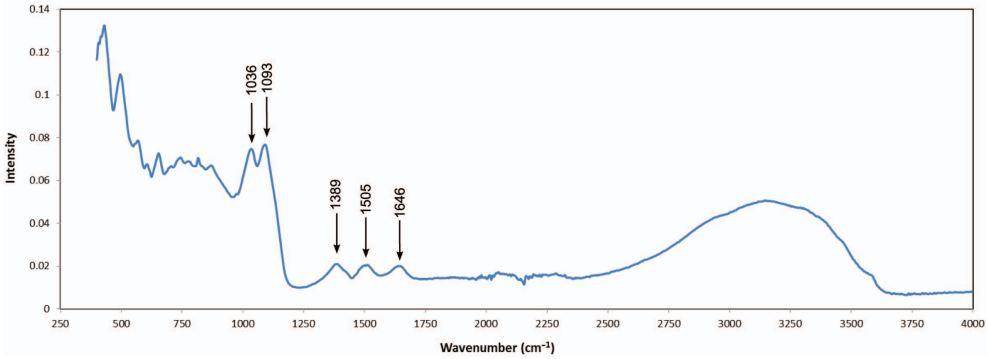


FIG. 3. IR spectrum for carbonatecyanotrichite (M50794) from the Grand View Mine, Coconino County, Arizona, USA. The bands at 1389 and 1505 $cm^{-1}$ were not present for cyanotrichite M50793 from the same locality.

ship between this mineral and khaidarkanite, clarifies the role of Sb in the camerolaite structure, and identifies a mode of accommodation for sulfate in the structure which is likely to operate in cyanotrichite as well. Thus, we not only verify that the cyanotrichite group is real, but now have a more detailed model for the structures of group members that have not yet become amenable to refinement. The differences between camerolaite and khaidarkanite structures also elucidate the types of short-range order and disorder that occur in these minerals, and explain why these structures have remained problematic for so long.

The camerolaite and khaidarkanite structures share the common structural feature of a three-wide ribbon of edge-sharing octahedra, with Al occupying the central octahedron and Cu in the two flanking octahedra, as proposed by Hager *et al.* (2009). These ribbons are clearly discernible in the structure of khaidarkanite (Fig. 4). The overall stoichiometry of this group is thus $Cu_2AlX_8$ or $Cu_4Al_2X_{16}$, where $X$ represents $OH^-$ and $H_2O$, or the oxygens of complex anions such as $SO_4^{2-}$. Similar triple octahedral ribbons are found in a modified form, corner-linked into continuous sheets, in the structure of parnauite, ideally $Cu_9(AsO_4)_2(SO_4)(OH)_{10}\cdot 7H_2O$ (Mills *et al.*, 2013).

In khaidarkanite, with monoclinic symmetry, the edge-sharing ribbons extend parallel to the unique crystallographic axis. Other members of the group, such as the camerolaite of this study, may be triclinic, but consistency is maintained by defining this direction as the *b* axis for all phases. The unit-cell repeat is very short in this direction: $b \approx 2.9$ Å. It is evident from the khaidarkanite and camerolaite structure refinements that this repeat corresponds to an average structure. The majority of sites in the structures that are not part of the ribbon defined above are only partly occupied, and it will be seen below that this must correlate with local ordering of occupied and vacant sites along the **b** direction, but that such one-dimensional order does not require order in other directions to form a supercell.

The close similarity between camerolaite and khaidarkanite cell dimensions is not immediately apparent from the data presented in Table 2, which were refined in a primitive triclinic cell. In order to facilitate a comparison between khaidarkanite, camerolaite and other members of the group, the camerolaite data are transformed into a *C*-centred cell which is the triclinic analogue of the *C*2/*m* khaidarkanite cell of Rastsvetaeva *et al.* (1997). The *b* and *c* axes are the same for *P* and *C* cells, but $\mathbf{a}_C = 2\mathbf{a}_P - \mathbf{b}_P$. The origin is also shifted by ½**c** from the ribbon Al site to approximately the same *z* coordinate as the Sb position (which corresponds to the non-ribbon Al2 site in khaidarkanite). The coordination transformation is thus $x_C = \frac{1}{2}x_P$, $y_C = y_P + \frac{1}{2}x_P$, $z_C = z_P + \frac{1}{2}$. This alternative cell for camerolaite has the space group *C*1, with the unit-cell parameters $a$ = 12.441(3), $b$ = 2.9130(6), $c$ = 10.727(2) Å, $\alpha$ = 93.77(3), $\beta$ = 95.57(3), $\gamma$ = 92.32(3)° and $Z = \frac{2}{3}$ (for a formula unit with 1 S and 1 Sb). Atomic coordinates for the *C*1 cell are shown in Table 5.

The edge-sharing ribbons in both refined structures stack in an *en echelon* fashion, but are shifted by *b*/2 relative to the adjacent ribbons on either side in the **a** direction. This allows the formation of strong hydrogen bonds O1–H1···O3 between neighbouring ribbons to form a corrugated layer of which the unit mesh is centred-

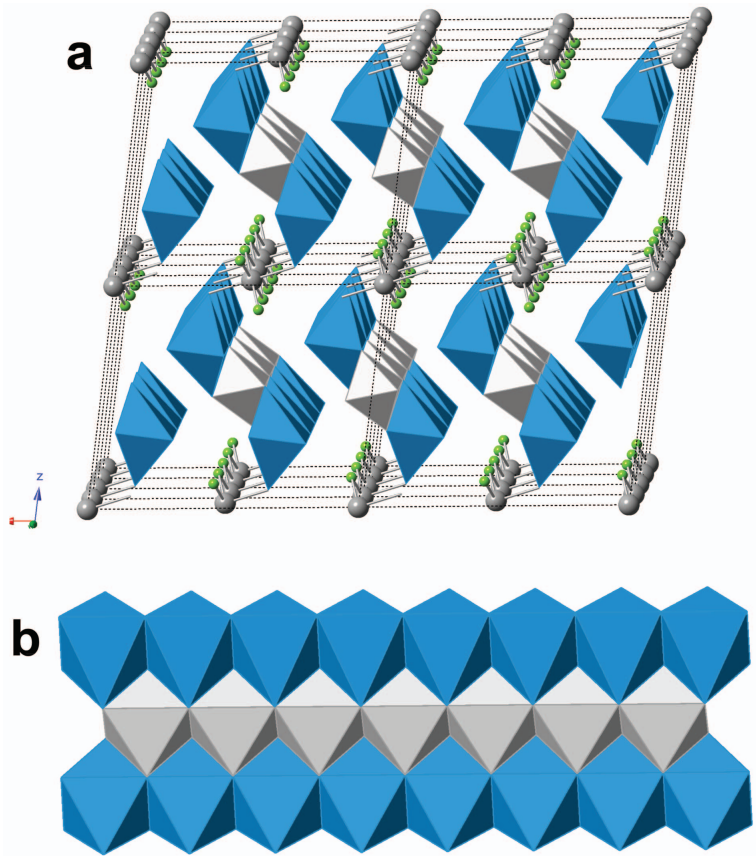


FIG. 4. (*a*) The average structure of khaidarkanite, viewed nearly down **b**. Blue octahedra in edge-sharing ribbons contain $Cu^{2+}$, grey octahedra contain $Al^{3+}$. Ribbons are cross-linked through additional partially occupied Al sites (grey spheres) and F (green). (*b*) An isolated $Cu_2Al(OH,H_2O)_8$ ribbon of khaidarkanite.

rectangular or nearly so (Fig. 5). This layer defines the *xy* plane of the structure. The vector **a** maps an atom in a ribbon to an equivalent atom in the next ribbon but one of the same layer. The layer of $Cu_4Al_2X_{16}$ ribbons is an invariant feature of all members of the group, so all have $a$ = 12.3−12.7 Å and $\gamma \approx 90°$. However, the crystal system may be monoclinic or triclinic, and *C*-centring may or may not be present. Representative unit-cell symmetries and lattice parameters in this axial setting are compared for all members of the group in Table 6.

### *Interlayer components of khaidarkanite and camerolaite*

The variation in composition, symmetry and unit-cell dimensions between members in the group arises because of the additional non-ribbon components. The composition of a hypothetical 'naked' ribbon with no such substituent would be $Cu_4Al_2(OH)_{14}(H_2O)_2$. In the structure of khaidarkanite, additional Al sites are present in the gaps between adjacent (001) layers of ribbons. These Al2 sites bridge the ribbons along the **c** direction by bonding to one $H_2O$ of the ribbon below and one $H_2O$ of the ribbon above. Octahedral coordination of Al2 is completed by four F, which are also in the interlayer gap. If the Al2 and F sites were fully occupied, they would form a continuous edge-sharing chain parallel to **b** of $AlF_4(H_2O)_2$ octahedra (Fig. 6*a*), and the resulting formula would be $Cu_4Al_2(OH)_{14}(H_2O)_2 + Al_2F_4$, with a net electrical charge of +2. However, the actual occupancies are 0.5 for Al2 and 0.75 for F, giving the observed electrostatically neutral

TABLE 5. Atomic coordinates for camerolaite for the *C*1 cell of the discussion.

| Site | Occupancy | *x* | *y* | *z* |
|---|---|---|---|---|
| Al | 1 | 0.4903 | 0.5293 | 0.4821 |
| Cu1 | 1 | 0.1541 | 0.5951 | 0.6807 |
| Cu2 | 1 | 0.3184 | 0.9474 | 0.2830 |
| O1 | 1 | 0.4305 | 0.4635 | 0.3078 |
| O2 | 1 | 0.0480 | 0.0550 | 0.6560 |
| O3 | 1 | 0.2200 | 0.4320 | 0.2778 |
| O4 | 1 | 0.2630 | 0.1170 | 0.6876 |
| O5 | 1 | 0.0775 | 0.5215 | 0.4574 |
| O6 | 1 | 0.3895 | 0.9985 | 0.5041 |
| O7a | 0.17 | 0.3285 | 0.8935 | 0.0310 |
| O7b | 0.17 | 0.3405 | 0.0705 | 0.0260 |
| O7o | 0.67 | 0.3090 | 0.9260 | 0.0470 |
| O8a | 0.17 | 0.4560 | 0.3360 | 0.9700 |
| O8b | 0.17 | 0.4255 | 0.5185 | 0.8760 |
| O8o | 0.67 | 0.4395 | 0.5305 | 0.8560 |
| O9a | 0.17 | 0.1145 | 0.1645 | 0.0870 |
| O9b | 0.17 | 0.0040 | 0.0510 | 0.0820 |
| O9o | 0.67 | 0.0490 | 0.0740 | 0.1020 |
| O10a | 0.17 | 0.0625 | 0.3475 | 0.8700 |
| O10o | 0.83 | 0.1235 | 0.5995 | 0.9050 |
| Sb | 0.33 | 0.4861 | 0.0031 | 0.9822 |
| S1 | 0.16 | 0.0710 | 0.9800 | 0.9600 |
| S2 | 0.17 | 0.4000 | 0.5050 | 0.0090 |

formula unit of $Cu_4Al_2(OH)_{14}(H_2O)_2$ + $(Al\square)_{\Sigma 2}(F_3\square)_{\Sigma 4}$ = $Cu_4Al_3(OH)_{14}(H_2O)_2F_3$. As Al2 must be surrounded by 4 F to complete an octahedron, simultaneous satisfaction of the requirements of electroneutrality, average site occupancies and Al coordination requires ordering of atoms and vacancies along any row of interlayer species || **b**. The ordering scheme that achieves this has Al octahedra occurring as edge-sharing dimers, so that $Al_2F_6$ groups are separated by two vacant Al and two vacant F sites (Fig. 6*b*). The *b* periodicity of the structure is thus quadrupled for the interlayer species. However, there is no constraint on the relative phases of ordering between different interlayer rows, so three-dimensional ordering does not occur, and no 4*b* superstructure is evident in Bragg diffraction, although layers of diffuse scattering might be expected to occur for $k$ = ¼-integral layers in reciprocal space. This behaviour is very similar to the one-dimensional ordering deduced for rods of $AsO_4^{3-}$ and $SO_4^{2-}$ groups in the structure of parnauite (Mills *et al*., 2013). Hager *et al*. (2009) note that khaidarkanite-like minerals could exist with different Al, F, OH and $H_2O$ contents, and it is clear that a range of such compositions could indeed be produced by varying the occupation patterns of the interlayer sites and the chemical speciation of the water content (OH or $H_2O$).

The average structure of camerolaite shows that Sb partially occupies interlayer octahedral sites that are analogous to Al2 in khaidarkanite. Note that $Sb^{5+}$ is found much more commonly in octahedral coordination than tetrahedral (Mills *et al*., 2009), although the camerolaite formula as originally written by Sarp and Perroud (1991) implied that Sb was present as tetrahedral $HSbO_4^{2-}$ replacing $SO_4^{2-}$. The sulfur of camerolaite partially occupies two distinct tetrahedral sites that alternate with Sb positions along the **b** direction, in contrast to the proposal by Hager *et al*. (2009) that the minor S content of khaidarkanite occupies the Al2 (≡ Sb) site. The positions of the S sites are shown in an idealized monoclinic version of the camerolaite average structure in Fig. 7*a*. Note that there are very short distances between Sb and S sites: Sb···S = 1.75−1.90 Å and S1···S2 = 2.24 Å according to the structure refinement. Furthermore, the $SbO_6$ octahedron shares faces with $SO_4$ tetrahedra, S1 and S2 tetrahedra share an edge, and $SO_4$ tetrahedra are linked through corners into

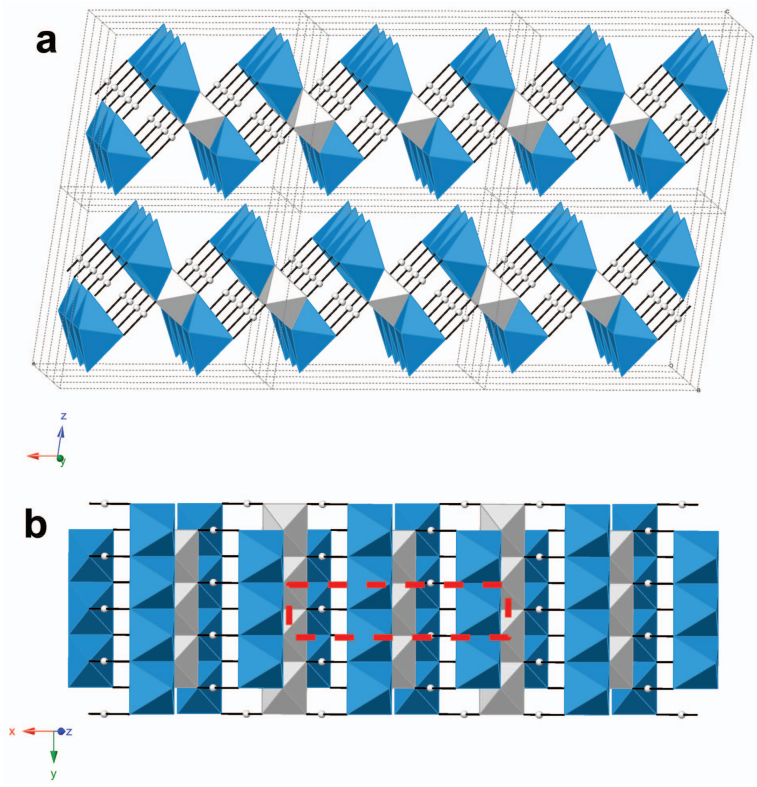


FIG. 5. Khaidarkanite structure with partially occupied sites omitted, showing the H bonds that link Cu–Al ribbons into layers parallel to (001). (*a*) Viewed nearly down **b**, as in Fig. 4; (*b*) a single layer viewed normal to (001), showing the offsets between successive ribbons that produce a centred-rectangular mesh in the *xy* plane (red dashed outline).

continuous chains || **b**. None of these features is physically realistic, so neighbouring cation sites cannot be occupied simultaneously. The principal constraints are: (1) if an Sb site is occupied, then the four nearest S sites must be vacant; and (2) if an S site is occupied, then the two nearest Sb must be vacant; and (3) if an S1 site is occupied, then the edge-sharing S2 must be vacant, or *vice versa*. The densest possible filling of Sb and S sites that is consistent with the 1:1 Sb:S ratio determined in this present study is that shown in Fig. 7*b*, where Sb, which bridges the top edge of one Cu−Al ribbon and the bottom of the next, alternates regularly with S bridging two Cu octahedra of either the bottom ribbon or the top ribbon. The average occupancy of the Sb site is ⅓ and that of the S sites is ⅙. The spacing of Sb atoms defines an incipient tripling of the structure periodicity along **b**, consistent with the diffuse streaking observed in diffraction, but note that sulfur randomly occupies either upwards-pointing tetrahedra (S1) or downwards-pointing tetrahedra (S2), and that there is no requirement for the Sb−S arrangements of neighbouring interlayer spaces to be in phase with one another. Thus, this is yet another structure in which a topologically unvarying matrix (of Cu−Al ribbons, in this case) hosts rods of intrinsically longer periodicity and disordered phase.

Accommodation of $[Sb(OH)_6]^-$ and $SO_4^{2-}$ groups in the structure of camerolaite requires adjustment of the numbers and locations of $OH^-$ and $H_2O$, which must be considered in order to derive an ideal formula for the mineral. Although H atoms were not located in the structure refinement, their location can be speculated on. The majority of anions in the Cu−Al ribbon must be $OH^-$ groups, and in the 'naked ribbon' $Cu_4Al_2(OH)_{14}(H_2O)_2$, the water molecules are expected to be the ligands with the weakest bonding to Cu or Al, namely those with only one long bond to Cu. In the 'naked ribbon', 50% of

TABLE 6. Space groups and examples of unit-cell parameters for members of the cyanotrichite group, transformed into the *C*-centred axial setting of this present study where necessary.

| Species | Space group | *a* (Å) | *b* (Å) | c (Å) | α (°) | β (°) | γ (°) |
|---|---|---|---|---|---|---|---|
| Khaidarkanite[1] | *C*2/*m* | 12.326(3) | 2.907(3) | 10.369(7) | 90 | 97.90(2) | 90 |
| Camerolaite[2] | *C*1 | 12.441(3) | 2.9130(6) | 10.727(2) | 93.77(3) | 95.57(3) | 92.32(3) |
| Camerolaite[3] | $P2_1/m$ or $P2_1$ | 12.527(8) | 2.903(2) | 10.756(6) | 90 | 95.61(4) | 90 |
| Cyanotrichite[4,5] | *P* monoclinic | 12.684(4) | 2.903(1) | 10.178(2) | 90 | 92.38(3) | 90 |
| Carbonatecyanotrichite[4,5] | *P* or *C* monoclinic | 12.551(6) | 2.833(4) | 10.166(6) | 90 | 98.61(8) | 90 |
| Cyanotrichite-like phase with Co≈Cu[4] | *P* or *C* monoclinic | 12.714(8) | 2.885(2) | 10.136(4) | 90 | 95.52(6) | 90 |
| Cyanotrichite-like phase from Clara Mine[4,6] | *P* or *C* monoclinic | 12.421(9) | 2.914(2) | 10.204(3) | 90 | 98.69(7) | 90 |
| | | 12.349(22) | 2.907(8) | 10.388(16) | 90 | 97.98(19) | 90 |

References: 1. Rastsvetaeva *et al.* (1997). 2. This study. 3. Sarp and Perroud (1991). 4. Hager *et al.* (2009). 5. Sample PAWCYAN, Museum Victoria catalogue number M50794, in which both species were intergrown. 6. Walenta (2001).

these ribbon-edge anions would be $OH^-$ and 50% would be $H_2O$. This is also true for khaidarkanite, where the ribbon-edge anions form part of the interlayer $AlF_4(H_2O)_2$ octahedra. Unlike Al2 of khaidarkanite, the interlayer cation Sb of camerolaite carries a formal valence of +5, and forms six bonds with an average bond valence of ⅚. This makes it unlikely that any of its ligands are water molecules, which have very low Lewis acidity. Instead, they are probably hydroxide anions, making the well-known $[Sb(OH)_6]^-$ anion that is found in minerals such as mopungite, $Na[Sb(OH)_6]$ (Williams, 1985), bottinoite, $[Ni(H_2O)_6][Sb(OH)_6]_2$ (Bonazzi and Mazzi, 1996) and the cualstibite group $[M_2^{2+}M^{3+}(OH)_6][Sb(OH)_6]$ with $M^{2+}$ = (Ni, Cu or Zn) and $M^{3+}$ = (Al or Fe) (Bonaccorsi *et al.*, 2007; Mills *et al.*, 2012*a*,*b*,*c*; Kolitsch *et al.*, 2013). To preserve electroneutrality, this anion must be incorporated by the net substitution $OH^- + H_2O \rightarrow [Sb(OH)_6]^-$, so the occupancy and positioning of Sb atoms will, to a degree, determine the arrangement of $OH^-$ and $H_2O$ in the ribbon edge. Accommodation of the sulfate groups also has consequences for the arrangement and proportions of $OH^-$ and $H_2O$, in that each $SO_4^{2-}$ tetrahedron can be envisaged as replacing two $OH^-$ on a ribbon edge, which must therefore be adjacent. In the occupation pattern of Fig. 7*b*, there are no ribbon-edge $OH^-$ that are not part of an $[Sb(OH)_6]^-$ octahedron, and the only remaining $H_2O$ are pairs that sit opposite each $SO_4^{2-}$ group across the interlayer. This arrangement has one $[Sb(OH)_6]^-$ and one $SO_4^{2-}$ per 6Cu, giving an ideal camerolaite formula of $Cu_4Al_2(OH)_{12}(H_2O)_{1.33}Sb(OH)_6]_{0.67}(SO_4)_{0.67}$, or $Cu_6Al_3(OH)_{18}(H_2O)_2[Sb(OH)_6](SO_4)$.

The relocated $H_2O$ is probably accommodated at one of the anion sites that is bound to only 2Cu and no Al, namely O3 or O4 of camerolaite, analogous to OH3 of khaidarkanite. It is interesting to compare this stoichiometry with the formula $Cu_4Al_2(HSbO_4,SO_4)(OH)_{10}(CO_3)\cdot 2H_2O$ proposed originally for type camerolaite from Cap Garonne, France, by Sarp and Perroud (1991). As $[Sb(OH)_6]^- + OH^-$ is chemically equivalent to $HSbO_4^{2-} + 3H_2O$, our formula could be expressed as $Cu_4Al_2(OH)_{11.33}[(HSbO_4)_{0.67}(SO_4)_{0.67}]_{\Sigma 1.33}\cdot 3.33H_2O$. The similarity is apparent, although our present study has significantly more S, Sb and $H_2O$, and no carbonate. The carbonate in the material of Sarp and Perroud (1991) was determined by CHN analysis. However, Raman spectroscopy of the holotype

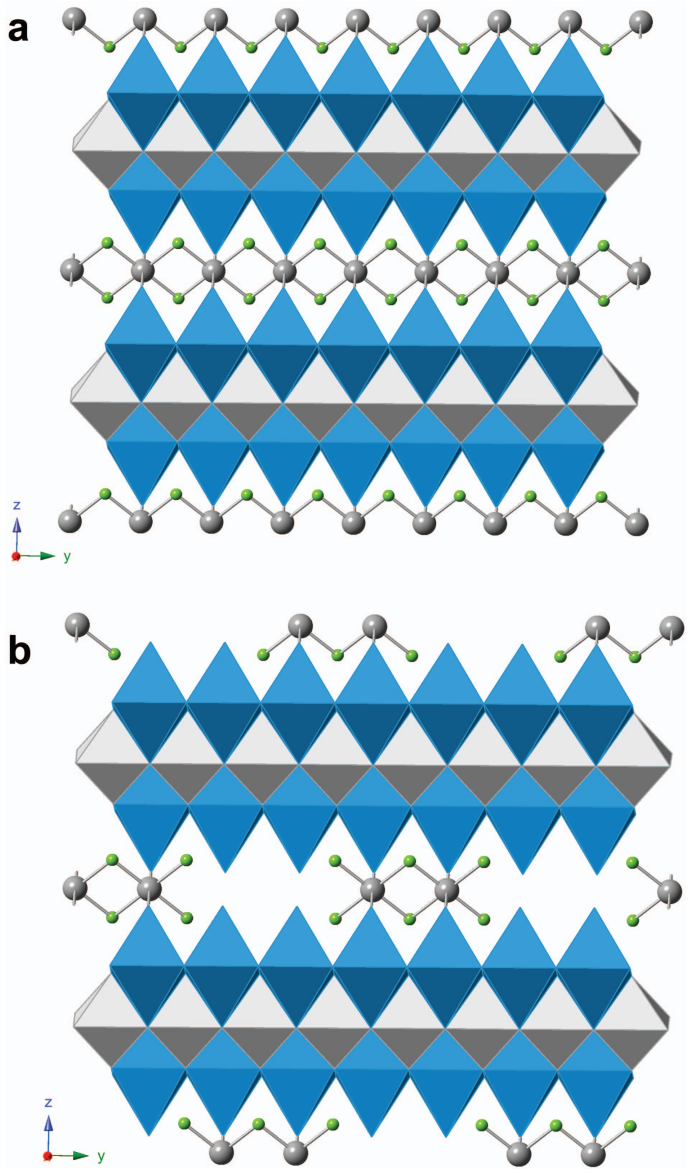


FIG. 6. (*a*) Ribbons of khaidarkanite viewed down **a**, showing bridges of partly occupied Al2 and F sites. (*b*) Long-range partial occupancies, electroneutrality and coordination requirements of Al2 are all satisfied if $Al_2F_6$ clusters alternate with two vacant Al sites and two vacant F sites along **b**, giving a local quadrupling of the b repeat. Different rows of interlayer species do not need to be in register with one another.

material and three other samples from Cap Garonne as well as camerolaite samples from other localities detected no carbonate bands (Table 1), and strong infrared bands unambiguously attributable to carbonate were seen only in Grand View mine carbonatecyanotrichite (Fig. 3). Therefore, we believe that the carbonate in the camerolaite analysis of Sarp and Perroud (1991) was due to inclusions or thin films of an impurity phase, as was found for parnauite by Mills *et al.* (2013). The empirical formula given by Sarp and Perroud, $Cu_{3.56}Al_{1.99}Sb_{0.59}S_{0.41}C_{0.99}H_{15.51}O_{19}$,

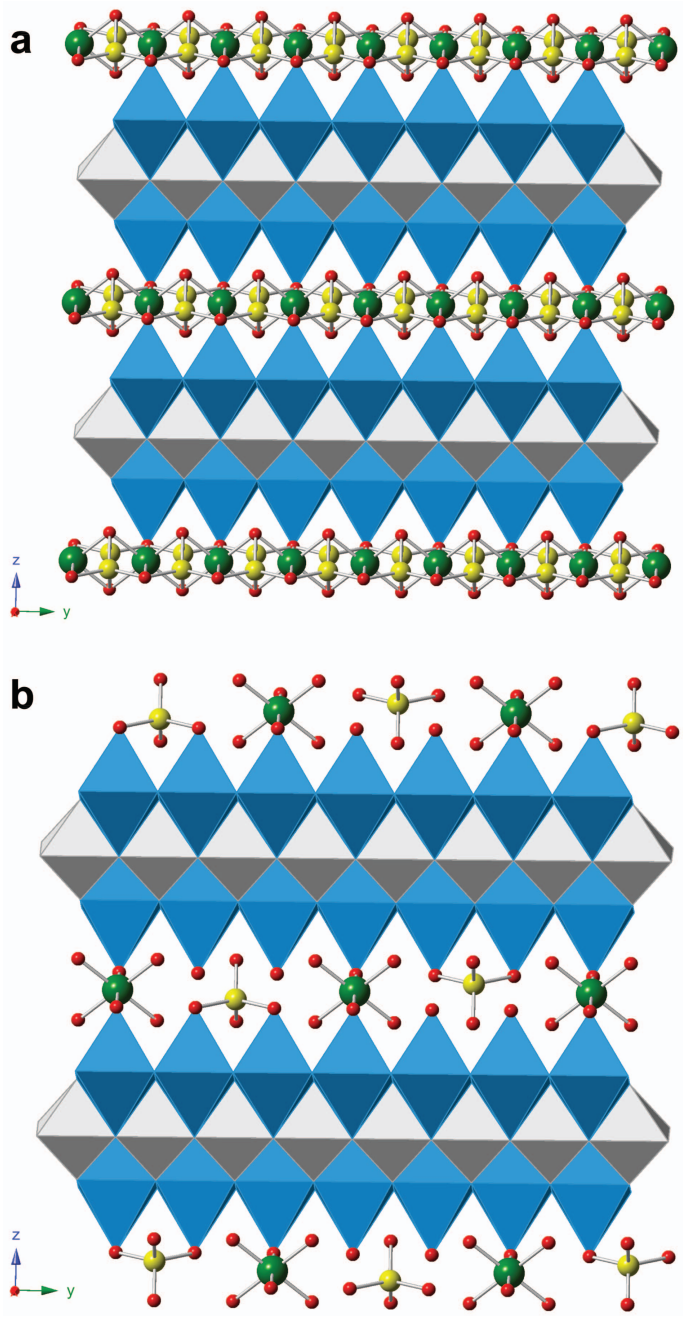


FIG. 7. (*a*) An idealized version of the camerolaite average structure, showing partially occupied Sb sites analogous to Al2 of khaidarkanite (green spheres) and S sites (yellow). Oxygen sites shown as red spheres are shared by $SbO_6$ octahedra and $SO_4$ tetrahedra. (*b*) Regular alternation of $SbO_6$ and $SO_4$ along **b** produces a local tripling of the structure periodicity. However, $SO_4$ tetrahedra point up or down randomly, and there is not necessarily any coupling in phase between successive interlayer rows.

can be recalculated to 6(Cu+Al) to give $Cu_{3.85}Al_{2.15}Sb_{0.64}S_{0.44}C_{1.07}H_{16.79}O_{20.53}$, with slight corrections to H and O in order to neutralize a −0.04 charge defect due to rounding errors. Note that the Sb content in this formula is now very similar (0.64 *vs*. 0.67) to that of our ideal formula $Cu_4Al_2(OH)_{12}(H_2O)_{1.33}[Sb(OH)_6]_{0.67}(SO_4)_{0.67}$. If $CO_2$ is eliminated and the remainder of the composition is rearranged analogously to our ideal formula, we obtain $Cu_{3.85}Al_{2.15}(OH)_{12.63}(H_2O)_{0.16}[Sb(OH)_6]_{0.64}(SO_4)_{0.44}$, which corresponds closely to our ideal formula but with substitutions of $0.15Al(OH)Cu_{-1}(H_2O)_{-1}$, $0.23(OH)_2(SO_4)_{-1}$, $0.03(OH)(H_2O)[Sb(OH)_6]_{-1}$, and a deficit of $1.05H_2O$ per 6(Cu+Al).

### *Variation in Sb and S content*

Walenta (1995) noted that the atomic Sb/S ratio was variable in camerolaite, ranging from 1.44 for the Cap Garonne type material to 0.64 at the Clara Mine, Germany. This may be due to low occupancies of one or both species, as in the recalculated Cap Garonne formula above. Alternatively, a range of Sb/S ratios could easily be generated through different sequences of Sb and S along the **b** direction in the interlayer, producing overall compositions intermediate between several endmembers.

Examples of these limiting structural arrangements and compositions are: (1) The 'naked' Cu−Al ribbon, with 50% $OH^-$ and 50% $H_2O$ at the ribbon edge, and no interlayer species. (2) A pattern in which isolated $[Sb(OH)_6]^-$ alternate with ($OH^-$ + $H_2O$) along **b** (Fig. 8*a*). (3) A band of continuous edge-sharing Sb octahedra along **b** (Fig. 8*b*). The need to form two bonds of valence ≈ ⅚ to Sb implies that the oxygens coordinated by two Sb is $O^{2-}$ rather than $OH^-$ or $H_2O$. Structures with finite sequences of edge-sharing Sb would correspond compositionally and structurally to intergrowths of (2) and (3). (4) A structure in which $SO_4^{2-}$ + $2H_2O$ repeat along **b**. The up/down sense of the sulfate tetrahedron is not ordered necessarily, but the minimum periodicity along any given sulfate chain is 2*b*. The corresponding composition is that of cyanotrichite, $Cu_4Al_2(OH)_{12}(SO_4)\cdot 2H_2O$, and this is a reasonable structure model for that mineral (Fig. 9*a*). Such a model is supported by the recent observation that cyanotrichite shows weak reflections corresponding to a 4*b* superstructure (F. Colombo, pers. comm., 2014), which would be obtained if the up/down sense of sulfates alternated regularly along each row. (5) Hager *et al*. (2009) speculated on the existence of a phase with twice the sulfate content of cyanotrichite, $Cu_4Al_2(OH)_{10}(SO_4)_2\cdot 2H_2O$. It is possible to realize such a composition if all ribbon-edge ($OH$ + $H_2O$) are replaced by sulfate oxygen atoms, with upwards- and downwards-pointing sulfate tetrahedra in a staggered configuration across the interlayer (Fig. 9*b*). There are no sites bonded to only one Cu available for the $H_2O$ molecules, but these can be transferred to the anion sites that are bonded to only two Cu and no Al (O3/O4 of the camerolaite structure presented here, or OH3 of the khaidarkanite refinement).

These possibilities are summarized in Table 7. Chemographically, compositions 1, 2 and 4−6 are all coplanar (Fig. 10). Endmember 3 is not a combination of the others, as it is equivalent to 2 (Endmember 2) − (Endmember 1) − $4H_2O$. Note that the ideal camerolaite composition corresponds to ⅔(Endmember 2) + ⅓(Endmember 5), although the local geometry around the sulfate anions is quite different from that in Endmember 5. Rather than encourage a potential proliferation of mineral names, it seems reasonable to apply the name 'camerolaite' to any material with a substantial Sb and S content where the Sb/S ratio is closer to 1:1 than to all-Sb or all-S compositions. The boundaries of a potential camerolaite field can thus be defined that includes a range of compositional and short-range ordering variants between Sb:S = 3:1 (Sb/S = 3) and Sb:S = 1:3 (Sb/S = ⅓). These limits include the full range noted by Walenta (1995) and are indicated by dashed lines in Fig. 10.

Sulfate groups that bridge adjacent $CuX_6$ octahedra of a ribbon edge, as found in this study, require considerable displacement and hence site splitting of the ribbon-edge anions. This is because the two oxygens that link Cu to S are translationally equivalent in the average structure, and are separated necessarily by $b \approx$ 2.9 Å, which is unrealistically long for the edge of a $SO_4$ tetrahedron. The grand average value for the sulfate S−O distance is 1.459 Å (Hawthorne *et al*., 2000), so the true O···O distance along the edge of a sulfate tetrahedron must be close to $\sqrt{(8/3)} \times 1.459 = 2.382$ Å. This implies that the sulfate oxygen atoms must displace away from their average positions towards the sulfur atom by ~±0.45 Å = 0.15*b*. This is an additional reason why two adjacent sulfur positions along the **b** direction cannot be occupied simultaneously, along with the need to avoid corner-linkage

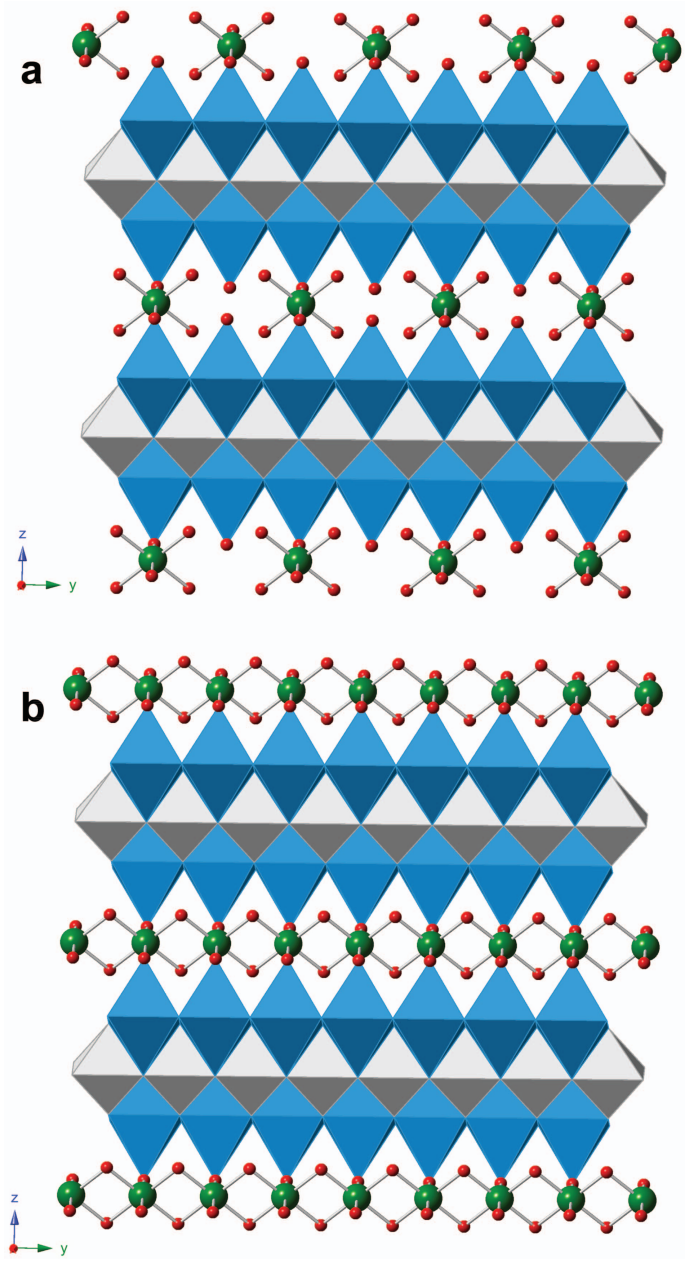


FIG. 8. (*a*) Idealized, hypothetical structure with discrete $[Sb(OH)_6]^-$ anions bridging Cu–Al ribbons, corresponding to endmember 2 of Table 7. (*b*) Structure with continuous edge-sharing chains $[Sb_2O_4(OH)_4]^{2-}$ between Cu–Al ribbons, corresponding to endmember 3 of Table 7. Cu octahedra are blue, Al octahedra grey, Sb atoms green and (OH,O) bonded to Sb are red.

between sulfate groups, which would overbond the bridging oxygen. In the current study, the O atoms affected are O7 (two of which bond to S2) and O10 (two of which bond to S1). The remaining O atoms of the sulfate groups, pointing into the interlayer, are O8 and O9 for both S1 and

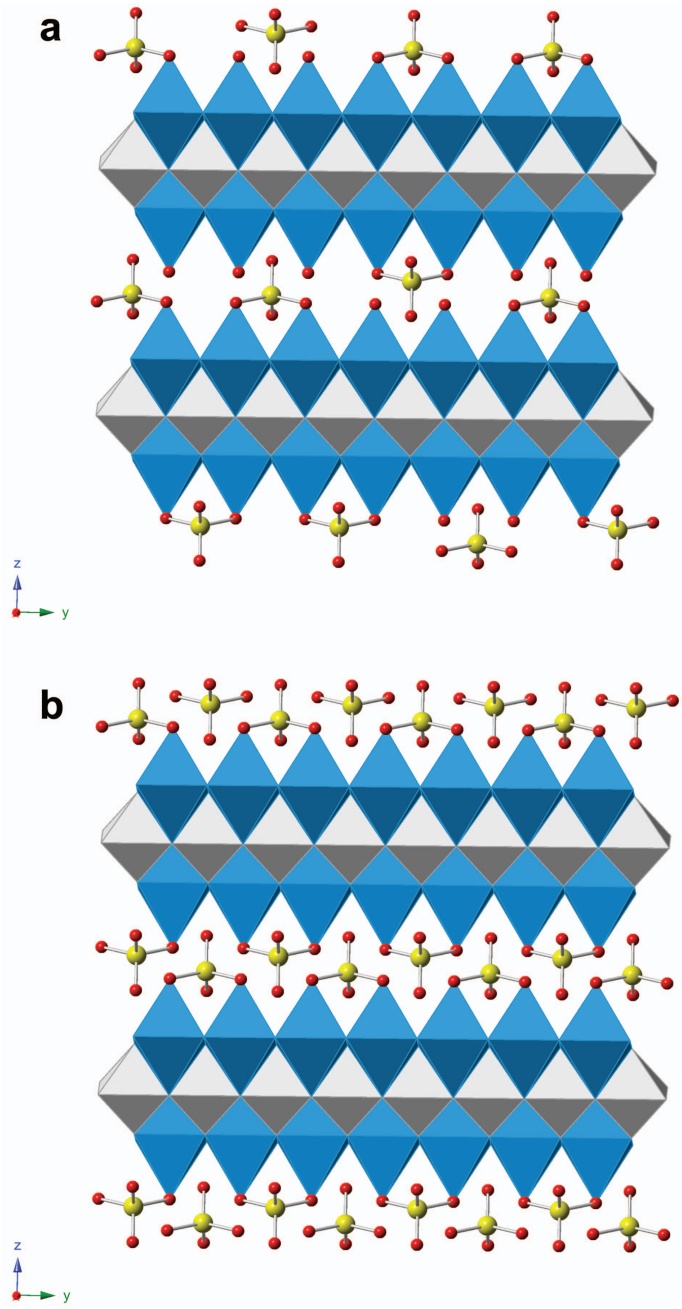


FIG. 9. (*a*) Idealized, hypothetical structure with $SO_4^{2-}$ anions attached randomly to the Cu–Al ribbon on the upper or lower side of the interlayer gap, corresponding to endmember 4 of Table 7. This model has the formula of cyanotrichite, and is proposed as the structure of that mineral. Regular up/down alternation of sulfate tetrahedra in every row would result in a 4*b* periodicity along the rows, while up/down disorder would give a 2*b* period. (*b*) Hypothetical structure with twice the $SO_4^{2-}$ content of cyanotrichite, corresponding to Endmember 5 of Table 7. The up/down sense of sulfate groups must alternate regularly along any given interlayer rod. Cu octahedra are blue, Al octahedra grey, S atoms yellow and sulfate oxygens are red.

TABLE 7. Summary of site occupancies and formulae for real and hypothetical (Sb,S)-bearing endmembers of the cyanotrichite group. Parameter $n$ = minimum interlayer periodicity in units of $b \approx 2.9$ Å.

| | Description/species | Invariant part of structure | O3/4 | Ribbon edge and interlayer | $n$ |
|---|---|---|---|---|---|
| 1 | Naked ribbon | $Cu_4Al_2(OH)_8$ | $(OH)_4$ | $(OH)_2(H_2O)_2$ | 1 |
| 2 | Isolated $[Sb(OH)_6]$ only | $Cu_4Al_2(OH)_8$ | $(OH)_4$ | $[Sb(OH)_6](OH)(H_2O)$ | 2 |
| 3 | Infinite chain of edge-sharing $[Sb(O,OH)_6]$ | $Cu_4Al_2(OH)_8$ | $(OH)_4$ | $[Sb_2O_4(OH)_4]$ | 1 |
| 4 | Cyanotrichite | $Cu_4Al_2(OH)_8$ | $(OH)_4$ | $(SO_4)(H_2O)_2$ | 2 |
| 5 | High-$SO_4$ phase | $Cu_4Al_2(OH)_8$ | $(OH)_2(H_2O)_2$ | $(SO_4)_2$ | 2 |
| 6 | Camerolaite | $Cu_4Al_2(OH)_8$ | $(OH)_4$ | $[Sb(OH)_6]_{0.67}[SO_4]_{0.67}(H_2O)_{1.33}$ | 3 |

S2, but again, each of these sites needed splitting in order to provide ligands around each S atom in a relatively regular tetrahedron of realistic size.

### *Site splitting of interlayer oxygen atoms*

As the occupancies of the two S sites in camerolaite are both only ⅙, the highest-occupancy components of the sites O7 and O10 are those which are not associated with sulfur, but which instead are $OH^-$ bonding to Sb or are $H_2O$. The corresponding split sites, labelled 'o' for 'original' (or 'octahedron'), had occupancies 66.7–83.3%, and their coordinates were refined normally. It is possible that these sites should be split further depending on whether they are occupied by $H_2O$ or $OH^-$, but investigation of this subtlety was not pursued in the current study (cf. discussion of the corresponding site in khaidarkanite by Hager *et al.*, 2009). Conversely, the split oxygen sites labelled 'a' and 'b' that bonded to sulfur had occupancies of

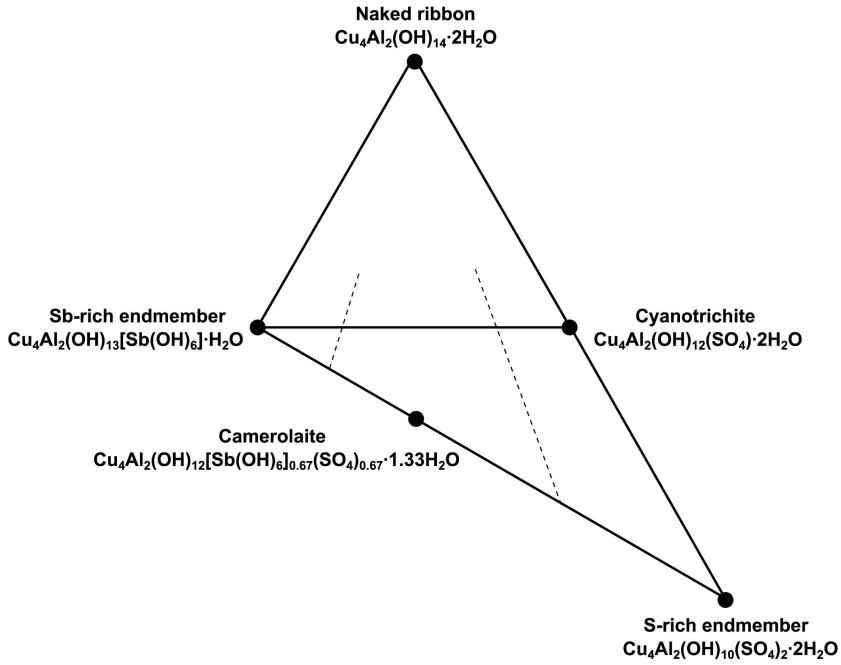


FIG. 10. Chemographic diagram showing relations between compositions of Table 7. Dashed lines indicate atomic Sb:S = 3:1 and 1:3, suggested as boundaries for the compositional field corresponding to the name camerolaite.

16.7%, corresponding to a scattering factor of only ~1.3 electrons, and their positions could not be refined robustly. Coordinates were therefore generated for them by manual iteration, starting from the corresponding 'o' positions, such that S−O distances were in the range 1.43−1.49 Å and the six tetrahedral edges O···O were 2.3−2.5 Å. One distance from S1 to O10o was found to be acceptable already (1.432 Å), so only one split site O10a had to be created in order to provide a ligand at the correct distance on the other side of the sulfur. For O7−O9, both 'a' and 'b' splits were needed. All 'a', 'b' and 'o' positions were fixed during final cycles of refinement. The average structure of camerolaite, showing the split sites, is shown in Fig. 11*a*, and a realization of the true local structure in Fig. 11*b*.

### *Symmetry reduction from C2/m to C1 in camerolaite*

The maximum possible space-group symmetry of camerolaite, as for all members of the cyanotrichite group, is the same as that of the layer of Cu−Al ribbons, namely *C*2/*m*. However, the actual structure as refined in this study has the lower symmetry *C*1. It has the only triclinic unit cell of those listed in Table 6. The principal causes of deviation from *C*2/*m* symmetry appear to be the following:

(1) The centred rectangular net of Fig. 5*b* is sheared to give angle $\gamma = 92.32^{\circ}$ rather than 90º (Table 6). This small shear is likely to be a secondary consequence of the relaxation of monoclinic symmetry constraints.

(2) Successive (001) layers of the structure are displaced relative to their neighbours parallel to **b**, because $\alpha = 93.77^{\circ}$ rather than 90º (Table 6). This displacement can be quantified as $c\cos\alpha = -0.705$ Å $= -0.242b$, and is visible in Fig. 11*b*. The closeness of this value to $b/4$ appears to be fortuitous, as there is no specific interatomic distance in the structure which would constrain it towards a rational fraction of *b*. This substantial shear may be required to optimize the H bonding between $[Sb(OH)_6]^-$, $SO_4^{2-}$ and $H_2O$ in the interlayer.

(3) Shear of the structure in the (100) plane does not seem to be driven by the need to accommodate large $Sb^{5+}$ cations in the interlayer. The octahedron around Sb is strongly distorted, with five Sb−O distances in the range 1.898−2.172 Å but the sixth (Sb−O10o) = 2.381 Å (Table 4). The bond-valence parameters of Mills *et al*. (2009) predict an average Sb−O distance of 1.982 Å for $Sb^{5+}$ in octahedral coordination, but <Sb−O> of 2.088 Å for the structure refinement of this study, giving a bond-valence sum of 4.16 valence units for Sb. The high degree of underbonding is reasonable, given the uncertainties involved in locating the oxygen atoms. The fact that the octahedron is distorted suggests that Sb would be even more underbonded in a more regular coordination environment, in accord with the Distortion Theorem (Allmann, 1975; Brown, 1978; Urusov, 2003). Therefore, factors other than the size of the Sb itself must be determining the size of the coordination polyhedron. The structural polarity affected by consistent orientation of the long Sb−O bonds is one of the main deviations from centrosymmetry in the structure.

(4) The bonding pattern of the sulfur atoms to O7 and O10 is polar along the **b** direction, causing loss of the potential mirror plane of symmetry. The S1 and S2 tetrahedra are also distinct from each other in orientation. There is potential for unequal occupation of the two S sites, but no significant difference was apparent in the refinement. It is likely that the controlling factor is interlayer H bonding.

The powder X-ray data of Sarp and Perroud (1991) are consistent with monoclinic rather than triclinic symmetry, and includes distinct reflections that violate *C*-centring, corresponding to $hkl = 011$, $21\bar{2}$, 212, $\bar{5}04$ and $\bar{2}14$ in our axial setting, and the third of these is quite strong ($I/I_{max} = 35\%$). On this basis, they deduced camerolaite to have space group $P2_1/m$ or $P2_1$ (Table 6), in contrast to our material. This suggests that the structural distortions associated with interlayer H bonding and accommodation of sulfate groups may couple together in more than one way. Cuchet (1995) reported another occurrence of camerolaite from Switzerland, but the space group remains unknown in the absence of diffraction data.

### *Descent in symmetry from C2/m for the cyanotrichite group*

We next examine the various degrees of structural freedom that arise in the descent from the ideal *C*2/*m* symmetry to its subgroups. Figure 12 uses stylized outlines of the khaidarkanite structure viewed down **b** (cf. Fig. 4*a*) to illustrate the additional degrees of freedom that are acquired as symmetry elements are lost. The Cu−Al ribbons are shown as parallelograms, with triangular

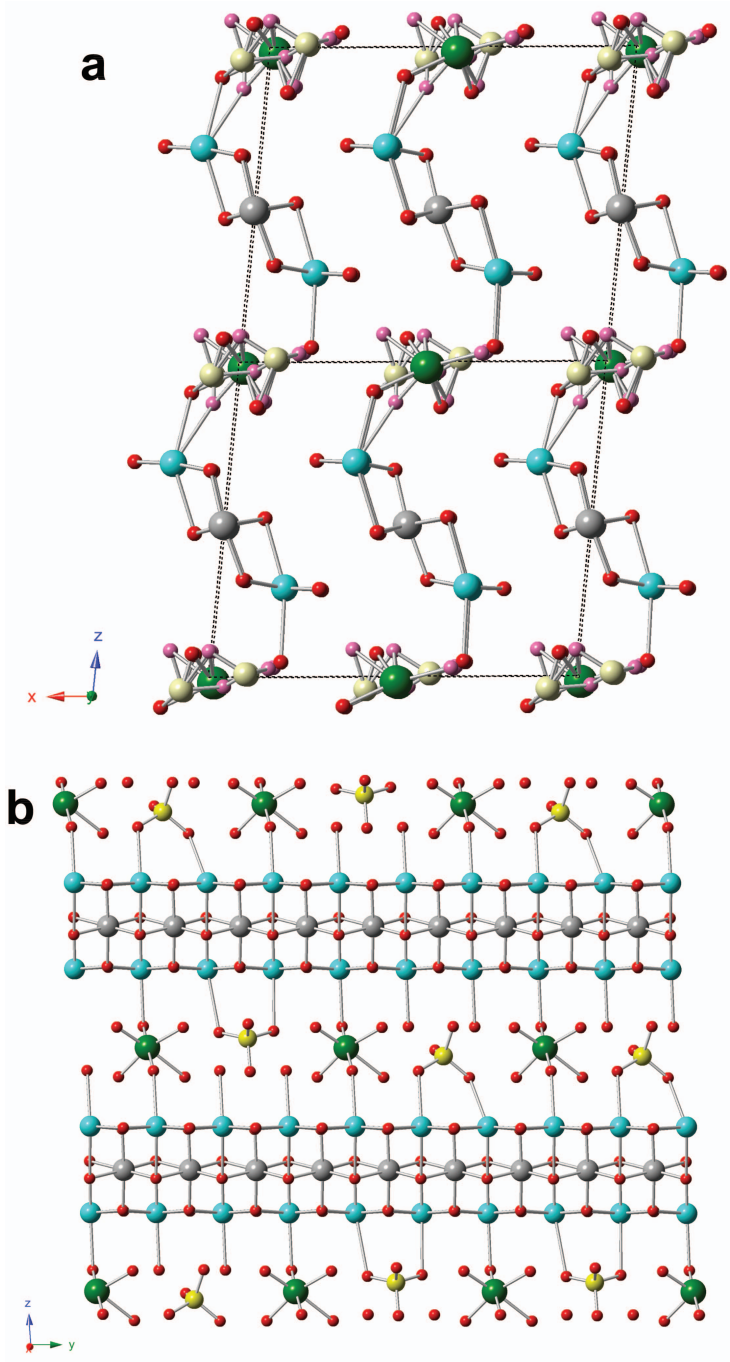


FIG. 11. (*a*) Average structure of camerolaite as refined in this present study, viewed down **b**. Al atoms are grey, Cu light blue, O red, Sb green. Low-occupancy (17−33%) split sites are O (pink) and S (light yellow). (*b*) A realization of the true structure viewed down **a**, showing alternation of Sb and S along **b** and offset of ~*b*/4 between the upper and lower Cu-Al ribbons. Compare with Fig. 7*b*.

decorations at the ends to represent ribbon-edge features such as sulfate tetrahedra or halves of Al/Sb octahedra. Maximally symmetrical ribbons carry no additional symbols. If a ribbon acquires a net polarity in the ±**b** direction, this is indicated by a '+' or '−' sign in a circle in the centre of the ribbon. If a ribbon acquires polarity in the ±**c** direction, this is indicated by a '↑' or '↓' sign in a circle. Ribbons that have lost their two-fold axis, mirror plane and centre of symmetry have both types of symbol superimposed. If a ribbon has $\bar{1}$ slab symmetry, then it is not polar overall, but may be sheared in the (100) plane, which is indicated by small '+' and '−' signs on the upper and lower triangles at the ribbon edges. The colour of the ribbons and triangles is generally grey, unless a ribbon has ±**c** polarity, in which case the symmetrical distinctness of the upper and lower ribbon edges is indicated by red and blue colours. In the case of space group *P*2/*m*, there are two completely independent ribbons per cell, which are also distinguished by red/blue colours. The cases that are considered are restricted to those *zellengleich* possibilities in which the unit cell remains ~12 Å × 3 Å × 10 Å, as observed for all minerals to date, but include: (1) *translationengleich* subgroups, in which the unit cell remains *C*-centred (Fig. 12*a*); (2) *klassengleich* subgroups, where the point symmetry remains 2/*m* but the Bravais lattice is primitive (Fig. 12*b*); and (3) the three cases with lattice type *P* and lower than 2/*m* point-group symmetry, but where all ribbons remain symmetry-related through centre of inversion, screw diad or *a*-glide operations (Fig. 12*c*).

It can be seen by inspection of Fig. 12*a* that the *C*1 space group of our camerolaite is associated with the ribbons acquiring polarity in both **b** and **c** directions, and all ribbons aligning parallel to one another. It is also apparent in Fig. 12*c* that the same number of degrees of freedom can be found in three *P* structures. *Pa* symmetry results if the **c** component of polarity remains ordered in a *ferro* fashion along the **a** direction, while the **b** polarity component alternates in an *antiferro* fashion. $P2_1$ symmetry corresponds to *antiferro* ordering of the **c** component combined with *ferro* ordering of the **b**, and $P\bar{1}$ to *antiferro* ordering of both polarity components. Hence, the $P2_1$ structure allows the same local relaxations as found for our camerolaite, but with the up/down sense of ribbon edges alternating along the **a** direction. This is therefore a likely structure model for the primitive monoclinic camerolaite of Sarp and Perroud (1991). The existence of both *C*1 and $P2_1$ structural variants of camerolaite, as well as fully symmetric *C*2/*m* khaidarkanite, implies that species of the cyanotrichite group may occur in more than one space-group variety, depending on the nature of ordering and distortion within the ribbons and ribbon edges, and how the ordering patterns couple between ribbons. All subgroup symmetries that have been determined to date are at least *zellengleich*, all being able to be indexed on a cell that is ~12.5 Å × 2.9 Å × 10.5 Å with β = 92−99º and other angles close to 90º (Table 6). However, any of the space groups shown in Fig. 12 could occur feasibly, with the possible exception of *P*2/*m*, which would require regular alternation of two completely symmetrically distinct types of ribbon along **a**.

## Compositional and structural variation in the cyanotrichite group

We are now in a position to enumerate the several independent types of compositional and structural variation and disorder that can occur in the cyanotrichite group.

### *Variation of interlayer content*

The different species known to date can be differentiated on the basis of the dominant species that are present in the interlayer and ribbon-edge regions. These are: $SO_4^{2-}$ tetrahedra in cyanotrichite, $[AlF_4H_2O)_2]^-$ octahedra in khaidarkanite, a 1:1 ordered combination of $SO_4^{2-}$ with $[Sb(OH)_6]^-$ in camerolaite, and $CO_3^{2-}$ triangles with subordinate $SO_4^{2-}$ in carbonatecyanotrichite. It is likely that $CO_3^{2-}$ in carbonatecyanotrichite can be accommodated at the ribbon edges by bridging two ribbon-edge anion sites, in the same way as $SO_4^{2-}$. The original carbonatecyanotrichite formula of Ankinovich *et al*. (1963) had a ratio $CO_3^{2-}$:$SO_4^{2-}$ of almost exactly 2:1, but it remains unknown whether or not there is ordering of the two anions. Hager *et al*. (2009) mooted the idea that the formula of Ankinovich *et al*. (1963) could be recalculated to give $[Cu_4Al_2(OH)_{12}][Al(OH)_3]_{0.49}(CO_3)_{0.7}(SO_4)_{0.3}\cdot 2H_2O$, in which excess Al is incorporated in the interlayer as a 'hydroxy-khaidarkanite' component, along with substantial carbonate and sulfate. It is apparent from the current study that a half-occupied interlayer Al site is not compatible with more than 0.5 (S+C) per formula unit, so this idea is no longer tenable. For now, it is assumed

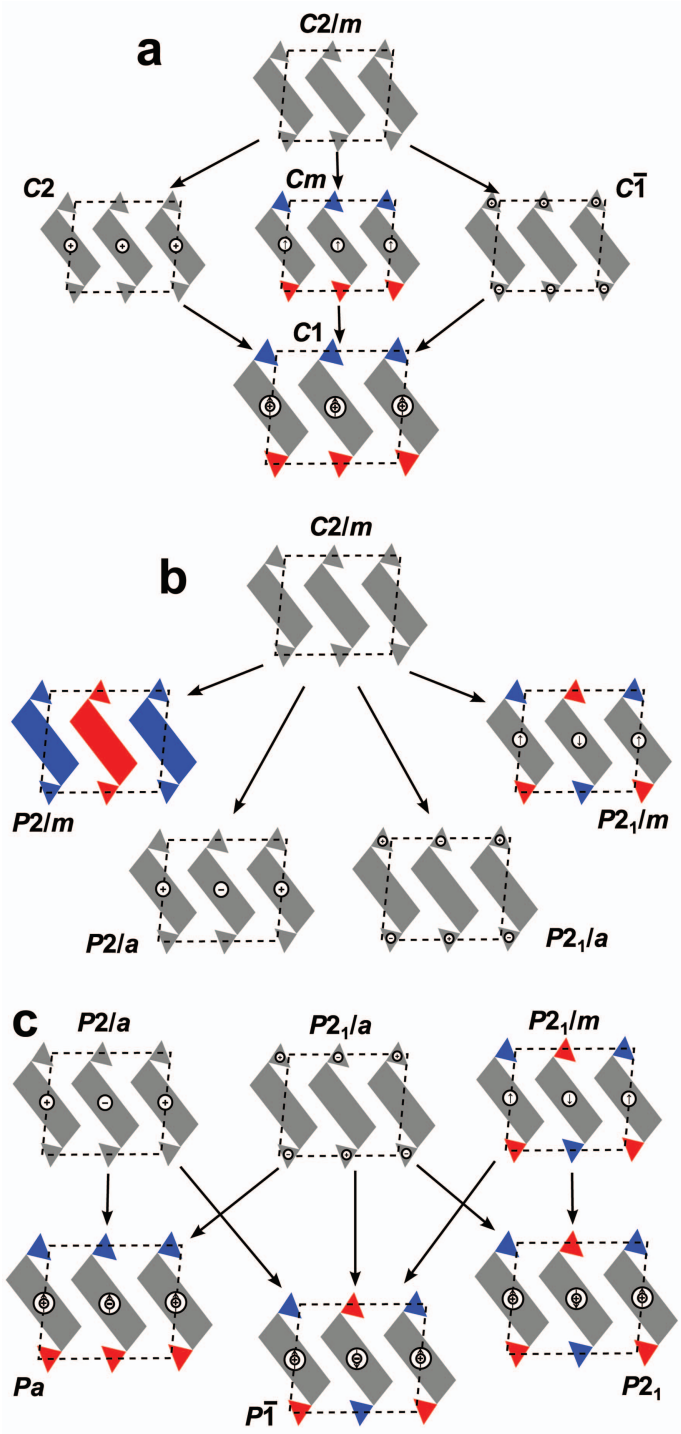


FIG. 12. The degrees of freedom gained through descent in symmetry from $C2/m$ to lower space groups. (*a*) *Translationengleich* subgroups that retain the *C*-centring. (*b*) *Klassengleich* subgroups with $2/m$ point group but a primitive lattice. (*c*) Deeper descent to $P2_1$, *Pa*, and $P\bar{1}$. Symbols and colours are explained in the text.

that carbonatecyanotrichite is the carbonate analogue of cyanotrichite with some $SO_4^{2-}$ replacing $CO_3^{2-}$. These different species, generated by substitution of variable interlayer components between constant ribbon layers are examples of merotypes (Makovicky, 1997; Chapter 1 in Ferraris *et al*., 2004).

It is interesting to note that, although minor sulfate has been found in khaidarkanite (Chukanov *et al*., 1999; Hager *et al*., 2009), and minor F in cyanotrichite (Sejkora *et al*., 2006), solid solution between cyanotrichite-group minerals appears to be very limited. Carbonatecyanotrichite and cyanotrichite can form intimate intergrowths in which the two phases give quite distinct sets of diffraction peaks (Hager *et al*., 2009), and both of these phases can coexist with khaidarkanite (Schnorrer and Bacher, 2000). Careful analysis of cyanotrichite-like minerals may uncover many more species with distinctive interlayer constituents, or ordered intermediates such as camerolaite.

### *Variation of ribbon content*

The ribbon cations are close to $Cu_4Al_2$ for all analyses to date, except for a brown, Co-rich cyanotrichite described by Hager *et al*. (2009). Only semi-quantitative analyses were available, but these suggested that Co $\approx$ Cu. If the symmetry is such that the ribbons are polar $\|$ **c**, with Cu1 and Cu2 sites symmetrically distinct, then such a composition could correspond to a new species if Co/(Co+Cu) > 0.25, with Co > Cu in one of the two Cu sites.

### *Variation of unit-cell symmetry*

As noted, relaxation of the ribbon and interlayer geometries may give rise to a range of subgroups of the maximal *C*2/*m* symmetry. However, this is not in general a species-defining feature of the structure. Fine intergrowth of more than one symmetry variant may contribute to the generally poor quality of diffraction from cyanotrichite-group minerals and the difficulty in characterizing their structures fully.

### *Local ordering along interlayer rods*

Ordered patterns of occupied and vacant sites along individual rod-like interlayer modules are required to reconcile long-range average site occupancies with short-range coordination and steric requirements in both khaidarkanite and camerolaite, as discussed in detail above. As the interlayer species are bonded to ribbon-edge anions, the local-ordering patterns are necessarily commensurate with $b \approx 2.9$ Å of the average structure, but require minimum periodicities of $4\times$ that distance for khaidarkanite, $3\times$ for camerolaite and $2\times$ for cyanotrichite ($4\times$ observed: F. Colombo, pers. comm., 2014). Thus, the structures of the cyanotrichite group consist of invariant host modules (layers of Cu–Al ribbons) in which are embedded rod-like units that have periodicity of an integral multiple of that of the host. Similarly, disordered rod-like units with local periodicities that are integral multiples of that of their host structure, have been deduced previously for the structure of parnauite (Mills *et al*., 2013).

Structures generated through the juxtaposition of two types of module with different translational symmetries are a special type of Order–Disorder (OD) family (Dornberger-Schiff, 1964; Ďurovič, 1997; Chapter 2 in Ferraris *et al*., 2004; http://www.crystallography.fr/math-cryst/OD_structures.htm). In general, OD analysis has been applied to structures which can be decomposed into layer-like modules, in which symmetries of individual layers and layer pairs differ. Ordering of the resultant distinguishable stacking operations normal to the layers can result in a series of polytypes. Two-dimensional polytypic variation involving translation of rod-like or prismatic structure modules, constitutes an extension to standard OD theory (Merlino *et al*., 2009), but has been described with translation on two symmetrically independent planes for the wollastonite–bustamite pyroxenoids (Angel, 1985) and fukalite (Merlino *et al*., 2009), and, with translation on two symmetry-related planes, relates the structure of $Li_2WO_4$-II to conventional spinelloids (Horiuchi *et al*., 1979; Christy and Zvyagin, 1994). These materials are composed entirely of the mobile structure modules, which interface with one another directly. Hence, long-range ordered stacking patterns are observed. However, in the structures of parnauite and the cyanotrichite group, the long-periodicity modules are separated from each other by the intervening host structure, so there is little driving force for phase coupling between interlayer rods in either the **a** or the **c** directions, and long-range order to form polytypic superstructures is unlikely to be observed. At most, a local period of $n\times b$ would be expected to produce diffuse scattering in the diffraction pattern at positions corresponding to $k = 1/n$ in reciprocal

space, as observed for the camerolaite of this study. Incommensurate and Vernier-commensurate cases of such 'one-dimensional columnar misfit' or 'host–guest' structures including sulfides, intermetallics and the $Hg_{3-x}[AsF_6]$ 'Alchemist's Gold' phase are reviewed in Hyde and Andersson (1989) and references cited therein. More recently, rather exotic examples of rods incommensurate with their host structure have been found in the high-pressure structures of Ba–IV (Nelmes *et al*., 1999) and a growing range of other chemical elements (Tse, 2005). Oxycompound examples in which incommensurate rods show limited phase coupling over distances of up to ~20 Å, resulting in layers of highly structured diffuse scattering in reciprocal space, were reported from non-stoichiometric apatite analogues by Christy *et al*. (2001).

The parnauite and cyanotrichite-group structures are an unusual type of host–guest structure in which the guest modules are necessarily commensurate in periodicity with the host structure, but phase coupling between guest modules is at best short-range.

### *Potential for stacking variation along z*

In monoclinic members of the cyanotrichite group, there is necessarily no offset in the **b** direction between successive (001) structural layers. However, the camerolaite of this study is triclinic, in which successive layers are displaced by a distance very close to $-b/4$. It is possible to imagine a unit-cell twinned version of such a structure in which such displacements alternate in sense $-b/4 + b/4 - b/4 + b/4$ along **c**, giving a unit cell with monoclinic symmetry and doubled periodicity along **c**. Such a structure would be another maximal-degree-of-order (MDO) member of a classical OD family, with layer-like structure modules. Indeed, polytypes generated by stacking vectors that are ±¼ of a lattice vector of the average structure are well known for minerals such as wollastonite (Henmi *et al*., 1983) and sapphirine (Dornberger-Schiff and Merlino, 1974; Christy and Putnis, 1988; Merlino and Zvyagin, 1998). However, no variation of this type has been noted in cyanotrichite-group minerals to date.

## Note on the occurrence and status of carbonatecyanotrichite

During the course of this study twelve samples were examined from the three museums in our search for good-quality examples of camerolaite, cyanotrichite and carbonatecyanotrichite. The last of these phases proved to be elusive. A sample labelled 'carbonatecyanotrichite', MHNG 443.027 (Engels mine, Plumas County, California, USA), was shown to be cyanotrichite, as was every example from the Cap Garonne mine. The only example of true carbonatecyanotrichite was M50794 from the Grand View Mine, Coconino County, Arizona, USA, where the mineral occurs with cyanotrichite as a separate phase that is quite distinct in XRD (Hager *et al*., 2009). Infrared analysis confirmed the presence of $CO_3$ in this sample, but not in cyanotrichite from the same locality. It is suspected that carbonatecyanotrichite is actually absent at Cap Garonne. Carbonatecyanotrichite therefore appears to be an extremely rare mineral. At most of its localities, cyanotrichite coexists with and predominates over it, and many 'carbonatecyanotrichite' specimens may in fact be misidentified cyanotrichite. As noted above, small amounts of carbonate in analyses may be due to the presence of minor impurity phases.

Note that there are ambiguities regarding the nature of carbonatecyanotrichite from the type locality. The powder XRD data of Ankinovich *et al*. (1963) agree well with those of carbonatecyanotrichite from other localities, including the specimen referred to as 'carbonatecyanotrichite' in the present study, and are distinct from those of true cyanotrichite (Hager *et al*., 2009). However, as reported in Pekov (1998), N.V. Chukanov analysed numerous specimens of 'carbonate-cyanotrichite' deposited in the Fersman Mineralogical Museum (Moscow) and Mining Museum of St. Petersburg, and found them to be intimate mixtures of a cyanotrichite and azurite. The cyanotrichite phase showed no significant carbonate content in IR and had close to 1 S per 6 (Cu+Al) (N.V. Chukanov, pers. comm., 2014). Thus, this mineral has a 'carbonatecyanotrichite' unit cell, but no carbonate content. Nevertheless, the present study has confirmed carbonate in Grand View mine material by IR spectroscopy. It is possible that the mineral may be a polytypic variety of cyanotrichite that can be stabilized by carbonate substitution, but that carbonate is not an essential constituent, in which case the species status of carbonatecyanotrichite must be regarded as questionable. Structural data are needed to confirm the role of carbonate in the structure and if it is essential in carbonatecyanotrichite.

## Acknowledgements

Reviewers Nikita Chukanov and Stefano Merlino are thanked for their constructive comments on the manuscript which helped to improve it greatly. Fernando Colombo is thanked for providing extra information on cyanotrichite. Nicolas Meisser and Stefan Ansermet (Musée Géologique Cantonal de Lausanne) are thanked for the loan of the samples from Les Moulins and Padern. Rosemary Goodall is thanked for help with obtaining the IR data. Pierre Clolus is thanked for taking the photomicrograph of the camerolaite sample.

## References

Allmann, R. (1975) Beziehungen zwischen Bindungslängen und Bindungsstärken in Oxidstrukturen. *Monatshefte für Chemie*, **106**, 779–793.

Angel, R.J. (1985) Structural variation in wollastonite and bustamite. *Mineralogical Magazine*, **49**, 37–48.

Ankinovich, E.A., Gekht, I.I. and Zaitseva, R.I. (1963) A new variety of cyanotrichite–carbonate-cyanotrichite. *Zapiski Vsesoyuznogo Mineralogicheskogo Obshchestva*, **92**, 458–463.

Anthony, J.W., Bideaux, R.A., Bladh, K.W. and Nichols, M.C. (2003) *Handbook of Mineralogy*. Volume V, Borates, Carbonates, Sulfates. Mineral Data Publishing, Tucson, Arizona, USA, 813 pp.

Berbain, C., Favreau, G. and Aymar, J. (2005) Mines et Minéraux des Pyrénées-Orientales et des Corbières. *Association Française de Microminéralogie*, 248 pp.

Bonaccorsi, E., Merlino, S. and Orlandi, P. (2007) Zincalstibite, a new mineral, and cualstibite: crystal chemical and structural relationships. *American Mineralogist*, **92**, 198–203.

Bonazzi, P. and Mazzi, F. (1996) Bottinoite, $Ni(H_2O)_6[Sb(OH)_6]_2$: crystal structure, twinning, and and hydrogen-bond model. *American Mineralogist*, **81**, 1494–1500.

Brese, N.E. and O'Keeffe, M. (1991) Bond-valence parameters for solids. *Acta Crystallographica*, **B47**, 192–197.

Brown, I.D. (1978) Bond valences – a simple structural model for inorganic chemistry. *Chemical Society Reviews*, **7**, 359–378.

Bruker (2001) *SADABS*. Bruker AXS Inc., Madison, Wisconsin, USA.

Christy, A.G. and Putnis, A. (1988) Planar and line defects in the sapphirine polytypes. *Physics and Chemistry of Minerals*, **15**, 548–558.

Christy, A.G. and Zvyagin, B.B. (1994) Polytypsim in minerals. Pp. 106–124 in: *Advanced Mineralogy V1: Composition, Structure and Properties of Mineral Matter: Concepts, Results and Problems* (A.S. Marfunin, editor). Springer-Verlag, New York.

Christy, A.G., Alberius-Hening, P. and Lidin, S.A. (2001) Simulation of diffuse scattering in non-stoichiometric apatites $Cd_{5-\eta/2}(VO_4)_3I_{1-\eta}$ and $Cd_{5-\eta/2}(PO_4)_3Br_{1-\eta}$: chimney-ladder structures with ladder-ladder and chimney-ladder coupling. *Journal of Solid State Chemistry*, **156**, 88–100.

Chukanov, N.V., Karpenko, V.Yu., Rastsvetaeva, R.K., Zadov, A.E. and Kuz'mina, O.V. (1999) Khaidarkanite, $Cu_4Al_3(OH)_{14}F_3{\cdot}2H_2O$, a new mineral from the Khaidarkan deposit, Kyrgyzstan. *Zapiski Vsesoyuznogo Mineralogicheskogo Obshchestva*, **128**, 58–63.

Cuchet, S. (1995) Seconde occurrence de camérolaïte, $Cu_4Al_2[(HSbO_4,SO_4)](OH)_{10}(CO_3){\cdot}2H_2O$, Val d'Anniviers, Valais, Suisse. *Schweizerische mineralogische und petrographische Mitteilungen*, **75**, 283–284.

Deliens, M., Berbain, C. and Favreau, G. (1993) *Les anciennes mines de Padern-Montgaillard (Aude) (Géologie, Histoire, Minéralogie)*. Association Française de Microminéralogie, Languedoc-Roussillon, France, 84 pp.

Dornberger-Schiff, K. (1964) *Grundzüge einer Theorie der OD Strukturen aus Schichten.* Abhandlungen der Deutschen Akademie der Wissenschaften zu Berlin, Kl. für Chemie, Geologie und Biologie, **3**. Berlin, 106 pp.

Dornberger-Schiff, K. and Merlino, S. (1974) Order-Disorder in sapphirine, aenigmatite and aenigmatite-like minerals. *Acta Crystallographica*, **A30**, 168–173.

Ďurovič, S. (1997) Fundamentals of OD theory. Pp. 3–28 in: *Modular Aspects of Minerals* (S. Merlino, editor). EMU Notes in Mineralogy Vol. **1**. Eötvös University Press, Budapest.

Favreau, G., Berbain, C. and Meisser, N. (2003) Cyanophyllite et autres minéraux rares de Padern (Aude). *Le Cahier des Micromonteurs*, **82**, 17–23.

Ferraris, G., Makovicky, E. and Merlino, S. (2004) *Crystallography of Modular Materials*. IUCr Monographs on Crystallography, **15**. Oxford University Press, UK, 370pp.

Hager, S.L., Leverett, P. and Williams, P.A. (2009) Possible structural and chemical relationships in the cyanotrichite group. *The Canadian Mineralogist*, **47**, 635–648.

Hawthorne, F.C., Krivovichev, S.V. and Burns, P.C. (2000) The crystal chemical of sulfate minerals. Pp. 1–112 in: *Sulfate minerals crystallography, geochemistry and environmental significance* (C.N. Alpers, J.L. Jambor and D.K. Nordstrom, editors). *Reviews in Mineralogy*, **40**. Mineralogical Society of America, Washington, DC.

Henmi, C., Kawahara, A., Henmi, K., Kusachi, I. and Takeuchi, Y. (1983) The 3*T*, 4*T* and 5*T* polytypes of wollastonite from Kushiro, Hiroshima Prefecture, Japan. *American Mineralogist*, **68**, 156–163.

Horiuchi, H., Morimoto, N. and Yamaoka, S. (1979) The crystal structure of $Li_2WO_4$-II: a structure related to spinel. *Journal of Solid State Chemistry*, **30**, 129–135.

Hyde, B.G. and Andersson, S. (1989) *Inorganic Crystal Structures*. Wiley-Interscience, New York, 430 pp.

Kabsch, W. (2010) *XDS*. *Acta Crystallographica*, **D66**, 125–132.

Kolitsch, U., Giester, G. and Pippinger, T. (2013) The crystal structure of cualstibite–1*M* (formerly cyanophyllite): its revised chemical formula and its relation to cualstibite–1*T*. *Mineralogy and Petrology*, **107**, 171–178.

Makovicky, E. (1997) Modularity – different types and approaches. Pp. 315–343 in: *EMU Notes in Mineralogy Vol. 1, Modular Aspects of Minerals* (S. Merlino, editor). Eötvös University Press, Budapest.

Merlino, S. and Zvyagin, B.B. (1998) Modular features of sapphirine-type structures. *Zeitschrift für Kristallographie*, **213**, 513–521.

Merlino, S., Bonaccorsi, E., Grabezhev, A.I., Zadov, A.E., Pertsev, N.N. and Chukanov, N.V. (2009) Fukalite: An example of OD structure with two-dimensional disorder. *American Mineralogist*, **94**, 323–333.

Mills, S.J., Christy, A.G., Chen, E.C.-C. and Raudsepp, M. (2009) Revised values of the bond valence parameters for $^{[6]}Sb(V)-O$ and $^{[3-11]}Sb(III)-O$. *Zeitschrift für Kristallographie*, **224**, 423–431.

Mills, S.J., Christy, A.G., Génin, J.-M.R., Kameda, T. and Colombo, F. (2012*a*) Nomenclature of the hydrotalcite supergroup: natural layered double hydroxides. *Mineralogical Magazine*, **76**, 1289–1336.

Mills, S.J., Christy, A.G., Kampf, A.R., Housley, R.M., Favreau, G., Boulliard, J.-C. and Bourgoin, V. (2012*b*) Zincalstibite-9*R*: the first 9-layer polytype with the layered double hydroxide structure-type. *Mineralogical Magazine*, **76**, 1337–1345.

Mills, S.J., Kampf, A.R., Housley, R.M., Favreau, G., Pasero, M., Biagioni, C., Merlino, S., Berbain, C. and Orlandi, P. (2012*c*) Omsite, $(Ni,Cu)_2Fe^{3+}(OH)_6[Sb(OH)_6]$, a new member of the cualstibite group from Oms, France. *Mineralogical Magazine*, **76**, 1347–1354.

Mills, S.J., Kampf, A.R., McDonald, A.M., Bindi, L., Christy, A.G., Kolitsch, U. and Favreau, G. (2013) The crystal structure of parnauite: a copper arsenate-sulphate with translational disorder of structural rods. *European Journal of Mineralogy*, **25**, 693–704.

Nelmes, R.J., Allan, D.R., McMahon, M.I. and Belmonte, S.A. (1999) Self-hosting incommensurate structure of Ba-IV. *Physical Review Letters*, **83**, 4081–4084.

Pekov, I.V. (1998) *Minerals First Discovered on the Territory of the Former Soviet Union*. Ocean Pictures, Moscow, 370 pp.

Rastsvetaeva, R.K., Chukanov, N.V. and Karpenko, V.U. (1997) The crystal structure of a new compound $Cu_4Al_3(OH)_{14}F_3(H_2O)_2$. *Doklady Akademii Nauk*, **353**, 354–357 [in Russian, English abstract: *American Mineralogist*, **83**, 188].

Sarp, H. and Perroud, P. (1991) Camerolaite, $Cu_4Al_2[HSbO_4,SO_4](OH)_{10}(CO_3)\cdot 2H_2O$, a new mineral from Cap Garonne mine, Var, France. *Neues Jahrbuch für Mineralogie, Monatshefte*, **1991**, 481–486.

Schnorrer, G. and Bacher, F. (2000) Die Mineralien von der Sonnblick-Nordwand, Rauris, Salzburg, Österreich – insbesondere der erste Khaidarkanit-Fund in Österreich. *Mineralien-Welt*, **11**, 52–57.

Sejkora, J., Ondruš, P., Fikar, M., Veselovský, F., Mach, Z., Gabašová, A., Škoda, R. and Beran, P. (2006) Supergene minerals from the Huber stock and Schnöd stock deposits, Krásno ore district, the Slavkovskýles area, Czech Republic. *Journal of the Czech Geological Society*, **51**, 57–101.

Sheldrick, G.M. (2008) A short history of *SHELX*. *Acta Crystallographica*, **A64**, 112–122.

Tse, J.S. (2005) Crystallography of selected high pressure elemental solids. *Zeitschrift für Kristallographie*, **220**, 521–530.

Urusov, V.S. (2003) Theoretical analysis and empirical manifestation of the distortion theorem. *Zeitschrift für Kristallographie*, **218**, 709–719.

Walenta, K. (1995) Camerolait aus dem Schwarzwald. *Aufschluss*, **46**, 210–214.

Walenta, K. (2001) Ein cyanotrichitähnliches Mineral von den Grube Clara. *Erzgräber*, **15**, 29–35.

Williams, S.A. (1985) Mopungite, a new mineral from Nevada. *Mineralogical Record*, **16**, 73–74.